SHAPE OPTIMIZATION
BY THE HOMOGENIZATION METHOD

Grégoire ALLAIRE
Commissariat à l'Energie Atomique
DRN/DMT/SERMA, C.E. Saclay
91191 Gif sur Yvette, France
& Laboratoire d'Analyse Numérique, Université Paris 6

Eric BONNETIER
Centre de Mathématiques Appliquées
Ecole Polytechnique
91128 Palaiseau, France

Gilles FRANCFORT
Institut Galilée
Université Paris-Nord
93430 Villetaneuse, France

François JOUVE
Centre de Mathématiques Appliquées
Ecole Polytechnique
91128 Palaiseau, France

Abstract

In the context of shape optimization, we seek minimizers of the sum of the elastic compliance and of the weight of a solid structure under specified loading. This problem is known not to be well-posed, and a relaxed formulation is introduced. Its effect is to allow for microperforated composites as admissible designs. In a two-dimensional setting the relaxed formulation was obtained in [6] with the help of the theory of homogenization and optimal bounds for composite materials. We generalize the result to the three dimensional case. Our contribution is twofold; first, we prove a relaxation theorem, valid in any dimensions; secondly, we introduce a new numerical algorithm for computing optimal designs, complemented with a penalization technique which permits to remove composite designs in the final shape. Since it places no assumption on the number of holes cut within the domain, it can be seen as a topology optimization algorithm. Numerical results are presented for various two and three dimensional problems.

Key words: homogenization, composite materials, optimal design, shape optimization, relaxation.

Contents

1 Introduction **3**

2 The original optimal design problem and its relaxed formulation. **4**

3 The relaxation process revisited. **11**

4 Explicit formula for the relaxed energy. **17**

5 A numerical algorithm for 2 and 3-dimensional shape optimization. **27**

5.1 description of the algorithm 27

5.2 A few technical algorithmic issues 29

6 Penalization of intermediate densities. **31**

7 Quasiconvexification versus convexification. **32**

8 Numerical results. **34**

8.1 The cantilever 1.6: 34

8.2 The bridge arch: 35

8.3 The 3-D cantilever 1.6: 35

8.4 The 3-D electric masts: 36

1 Introduction

Shape optimization is a major issue in structural design. One of the most challenging aspects of shape optimization is what structural engineers refer to as the layout, or topology, optimization. Classical methods of shape optimization, based on boundary motion, are ill equiped to capture the possible topological complexity of the shape because the required smoothness assumptions on the boundary of the material domain do not permit hole punching, although it is widely acknowledged that creating holes (*i.e.*, changing the topology) may drastically improve the performance of a candidate optimal shape.

In theory the remedy is straightforward: allow for holes of any shape and any size within the design region. The recipe is deceptive because the issue at stake is truly of a mathematical nature. The collection of admissible holes should be such that meaningful optimality criteria can be proposed. If, as will be the case in the remainder of the paper, the announced goal is to minimize the compliance of an elastic structure under a weight constraint, the optimization process is really a bang-bang problem (material or void) in an infinite dimensional space, say that of characteristic functions of the shape: a well known difficulty since the work of Pontryaguin. The resulting formulation is generically ill-posed. The reader is refered to the typical counter-examples presented in [31] for model problems of control through the coefficients of an objective functional depending on the solution of a linear partial differential equation.

It is well known since the pioneering work of Murat and Tartar [33] that a larger class of admissible designs must be introduced. The adequate class to be considered is precisely the concern of the theory of homogenization. Here again the seminal idea is straightforward: allow for fine mixtures of void and material on a scale which is much smaller than the mesh used for the actual computation. In physical terms admissible designs should now include arbitrary microperforations of the elastic material within the design domain. Of course there are many microstructures that correspond to the same volume fraction of void in a porous medium and the generalized designs are characterized not only by the volume fraction of void but also by the resulting effective tensor (or Hooke's law) which depends in turn on the specific microgeometry. Unfortunately, the set of effective tensors resulting from the mixture in fixed volume fraction of two elastic materials is unknown, although its conductivity analogue is known [33]. This obstacle is alleviated in the particular case where the objective functional is the elastic compliance because its minimum can be computed among a well-known subset of the full set of effective tensors, namely that of sequential laminates.

This process of enlarging the space of admissible designs in order to get a well posed problem is called relaxation. The intimate connection between relaxation and homogenization is demonstrated in [33] for a scalar setting. In a context closer to that of shape optimization, it is explored at length in [26]. Bona fide shape optimization imposes an additional hurdle: one of the phases in the mixing process is actually degenerate. Homogenization theory is crippled by the presence of material voids and, although formal computations suggest as a placebo the filling of holes with a very compliant material, a full mathematical justification is still pending.

The present paper should be approached within such a background. On the one hand we carefully map the passage from the original shape optimization problem to its assumed relaxed formulation. This permits to prove satisfactory, albeit partial, relaxation results in two, as well as three, dimensions. On the other hand we squeeze the relaxed formulation for every drop of available information and propose a new computational algorithm for two and three dimensional shape optimization that takes full advantage of the thorough knowledge of the optimal microstructures. In some sense, this paper can be seen as a continuation and a generalization of [6] which was a purely two dimensional work.

The importance of the homogenization method for shape optimization goes far beyond proving existence theorems for relaxed optimal designs and establishing necessary conditions of optimality. Since the work of Bendsoe and Kikuchi [11], a new class of numerical algorithms based on the homogenization method has appeared. They are frequently viewed as "topology optimization" algorithms since they are able to capture very fine patterns of the optimal shape on a fixed numerical grid. Our algorithm belongs to this class and is the first one to use optimal microstructures in three dimensional computations. Other numerical applications of the homogenization method for shape optimization may be found in [2], [4], [9], [10], [13], [24], [25], [36], and [40].

In Section 2 we carefully state the original shape optimization problem as well as the relaxed problem investigated thereafter. Section 3 is a step by step exploration of the relaxation process; we demonstrate that the hole filling process results in a formulation which is indeed a likely candidate although a complete relaxation result is wanting (see Theorem 3.1 and Proposition 3.2). Section 4 details the intimate properties of the relaxed energy and in particular the type of optimal microstructure (multiple layers) and the values of the associated parameters (the directions and volume fractions in each layering process). The ensuing algorithm is presented in Section 5: it is an alternate direction algorithm which successively computes the stress field through the solving of a problem of linear elasticity and the optimal microstructure for that stress field. Section 6 is devoted to some *ad hoc* penalization techniques that will extract sound classical designs out of unfeasible generalized designs. Section 7 is a discussion of the merits of the fictitious material approach broadly used in shape optimization. It is shown on a typical example to yield a worse design than the homogenization method. Section 8 presents our numerical results: 2-D and 3-D computations are displayed.

As a final note, the reader may find the paper somewhat unsettling to the extent that it addresses issues ranging from mathematical proofs of existence of relaxed solutions all the way to numerical treatments of various parameters in our 2-D and 3-D finite element code. Our decision to tackle such a broad spectrum of issues is anchored in our belief that only a detailed knowledge of shape optimization will permit further progress in theory as well as in numerical practice.

2 The original optimal design problem and its relaxed formulation.

Consider a bounded domain Ω in $I\!R^N$ subject to "smooth enough" surface loadings f (e.g. $f \in H^{-1/2}(\partial\Omega)^N$) on its boundary $\partial\Omega$. We assume global equilibrium of this surface loadings, *i.e.*,

$$\int_{\partial\Omega} f ds = 0.$$

Part of the domain is occupied by an isotropic linearly elastic material with elasticity

$$A = (\kappa - \frac{2\mu}{N})I_2 \otimes I_2 + 2\mu I_4, \quad 0 < \kappa, \mu < +\infty, \tag{1}$$

while the remaining part of Ω is void. Let χ denote the characteristic function of the part Ω_χ of Ω occupied by the elastic material. Whenever Ω_χ is a smooth enough open subdomain of Ω such that $\partial\Omega_\chi$ contains the part of $\partial\Omega$ where f is non zero, the elasticity problem in Ω_χ is well-posed, *i.e.*, the following set of equations

$$\begin{cases} \sigma = Ae(u) & e(u) = 1/2\,(\nabla u + \nabla^t u)\,, \\ div\ \sigma = 0 & \text{in } \Omega_\chi, \\ \sigma \cdot n = f & \text{on } \partial\Omega_\chi \cap \partial\Omega, \\ \sigma \cdot n = 0 & \text{on } \partial\Omega_\chi \setminus \partial\Omega. \end{cases} \tag{2}$$

has a unique solution $u \in H^1(\Omega_\chi)^N$ (up to a rigid displacement field). Here, u is the displacement vector and σ is the associated Cauchy stress field uniquely defined in $L^2(\Omega_\chi; I\!R_s^{N^2})$.

As such σ can be extended to an element of $L^2(\Omega; I\!R_s^{N^2})$ which further realizes the minimum of the complementary energy over all statically admissible stress fields, *i.e.*,

$$c(\chi) := \int_\Omega A^{-1}\sigma \cdot \sigma dx = \min_{\tau \in \Sigma(\chi)} \int_\Omega A^{-1}\tau \cdot \tau dx \tag{3}$$

where the set $\Sigma(\chi)$ is defined by

$$\Sigma(\chi) = \left\{ \tau \in L^2(\Omega; I\!R_s^{N^2}) \mid div\ \tau = 0 \text{ in } \Omega;\ \tau \cdot n = f \text{ on } \partial\Omega;\ \tau(x) = 0 \text{ a.e. where } \chi(x) = 0 \right\}. \tag{4}$$

The quantity $c(\chi)$, defined by (3), is called the compliance of the body and a straightforward integration by parts demonstrates that

$$c(\chi) = \int_{\partial\Omega} f \cdot u dx,$$

where u is the solution of (2).

When $\chi(x)$ is the characteristic function of an arbitrary measurable subset of Ω (not necessarily open) the existence of σ is no longer guaranteed. A generalized compliance may however be defined as

$$c(\chi) := \inf_{\tau \in \Sigma(\chi)} \int_\Omega A^{-1}\tau \cdot \tau dx \tag{5}$$

with $\Sigma(\chi)$ defined by (4) (note that the infimum is not necessarily attained).

The goal of optimal design is to devise the least compliant structure compatible with the loads for a given weight of the structure. Thus, the range of compliances $c(\chi)$ for all characteristic functions χ such that

$$\int_\Omega \chi(x) dx = \Theta, \quad 0 < \Theta \le |\Omega|,$$

is investigated and the optimal design problem reads as

$$I := \inf \left\{ c(\chi) \ \mid \ \chi \in L^\infty(\Omega; \{0,1\}); \ \int_\Omega \chi(x) dx = \Theta \right\}. \tag{6}$$

The optimal design problem defined in (6) is difficult to handle since it is constrained by

$$\int_\Omega \chi(x) dx = \Theta. \tag{7}$$

Such a constraint is routinely handled in elementary calculus of variations through the introduction of a positive Lagrange multiplier. Thus, (6) is replaced by

$$I(\ell) := \inf_{\chi \in L^\infty(\Omega;\{0,1\})} \left\{ c(\chi) + \ell \int_\Omega \chi(x) dx \right\}, \tag{8}$$

in the hope that there exists a positive value of ℓ for which the volume constraint (7) is met. That it is so is not obvious in the case at hand, and as such it should be justified. We are unfortunately helpless in the matter as will be further pointed out at the end of Section 3 below. Thus, we content ourselves with the above unconstrained version of the original optimization problem.

Remark 2.1 *For the sake of simplicity we consider only the case where surface loads are applied. A straightforward modification of the model would however permit the consideration of volume forces or the clamping of part of the boundary $\partial\Omega$ (*i.e.*, the enforcement of a Dirichlet boundary condition $u = 0$). The reader is referred to the numerical examples presented in Section 8 which include different types of boundary conditions.*

Remark 2.2 *The above optimization problem is usually referred to as a "single load" problem. This means that the elastic structure is optimized for a single configuration of loading forces and may well be totally inadequate for other loads. In practice it is an undesirable feature and it is quite often more realistic to investigate the so-called "multiple loads" problem which amounts to an optimization of the structure for several configurations. Specifically, various surface loadings $f_1, \cdots, f_p$ are given and we consider the minimization problem*

$$I_p(\ell) := \inf_{\chi \in L^\infty(\Omega;\{0,1\})} \left\{ \sum_{i=1}^p c_i(\chi) + \ell \int_\Omega \chi(x) dx \right\} \tag{9}$$

where $c_i(\chi)$ is the generalized compliance defined by (5) for the boundary condition f_i. Most of the obtained theoretical results hold true for the multiple loads problem. For the sake of brevity, the article is structured around the single load case; the multiple loads case is only mentioned when it departs from its single load analog. Remark, however, that the numerical algorithm for the multiple loads problem is more complex than that of the single load case since an explicit formulation of the relaxed problem (in other words an explicit formula for the optimal microstructure) is not available.

It is well-known since the seminal counter-examples of Murat [31] that problems of the type (6) or (8) are generically ill-posed to the extent that minimizers need not exist among characteristic functions. The problem must be relaxed, and the optimum is achieved by a generalized design which involves infinitely fine micro-perforations of the material. A simple and concise description of the relaxation process in the present setting may be found in [6]; it is briefly recalled below.

In a first step, a convenient rewriting of $I(\ell)$ is achieved as follows. Choose an arbitrary characteristic function χ in $L^\infty(\Omega;\{0,1\})$. If τ is an admissible test stress field in the definition (5) of the compliance $c(\chi)$, the set $\{x\in\Omega \mid \tau(x)=0\}$ is measurable and it contains the set $\{x\in\Omega \mid \chi(x)=0\}$. But clearly, if $\tilde{\chi}$ is the characteristic function of the complement in Ω of $\{x\in\Omega \mid \tau(x)=0\}$, then

$$\int_\Omega \left(A^{-1}\tau\cdot\tau+\ell\tilde{\chi}\right)dx \le \int_\Omega \left(A^{-1}\tau\cdot\tau+\ell\chi\right)dx,$$

so that $I(\ell)$ is equivalently defined by

$$I(\ell)=\inf_{\chi,\tau}\left\{c(\chi)+\ell\int_\Omega \chi(x)dx\right\}, \tag{10}$$

where $\chi\in L^\infty(\Omega;\{0,1\})$ and $\tau\in L^2(\Omega;I\!R_s^{N^2})$ are now constrained by

$$\begin{cases} div\ \tau=0 & \text{in } \Omega \\ \tau\cdot n=f & \text{on } \partial\Omega \\ \tau(x)=0 \text{ if and only if } \chi(x)=0 & \text{a.e. in } \Omega. \end{cases} \tag{11}$$

After minimization in χ,

$$I(\ell)=\inf_{\tau\in\Sigma(\Omega)}\int_\Omega f_\ell(\tau)dx, \tag{12}$$

where

$$\Sigma(\Omega):=\left\{\tau\in L^2(\Omega;I\!R_s^{N^2}) \ \mid\ div\ \tau=0 \text{ in } \Omega;\ \ \tau\cdot n=f \text{ on } \partial\Omega\right\}, \tag{13}$$

and

$$f_\ell(\tau):=\begin{cases} 0 & \text{if } \tau=0 \\ A^{-1}\tau\cdot\tau+\ell & \text{if } \tau\neq 0. \end{cases} \tag{14}$$

The function f_ℓ defined in (14) combines two pathologies: lack of convexity and lack of continuity at the origin. The lack of convexity (or even quasi-convexity) is by now a usual feature of vector-valued minimization problems and it calls for a relaxation of f_ℓ. The lack of continuity of f_ℓ at $\tau=0$ is the mathematical manifestation of the presence of holes in Ω. It is physically reasonable and, as will be seen later, mathematically sound to fill the holes with a very compliant material η. In other words, for small η, f_ℓ is approximated by

$$f_\ell^\eta(\tau):=\min\left\{A^{-1}\tau\cdot\tau+\ell,\eta^{-1}\tau\cdot\tau\right\}. \tag{15}$$

Note that, as η (the stiffness of the ersatz material) tends to zero, the sequence of functions f_ℓ^η monotonically converges to f_ℓ.

In a second step, the relaxation process is performed at fixed η. Thus, (12) is replaced by

$$I(\ell,\eta)=\inf_{\tau\in\Sigma(\Omega)}\int_\Omega f_\ell^\eta(\tau)dx. \tag{16}$$

The relaxation of (16) is well understood. The reader is referred to [6] for a detailed exposition of the method (see also [5] for many technical details). The result is

$$I(\ell,\eta) = I^*(\ell,\eta) := \min_{\tau\in\Sigma(\Omega)} \int_\Omega F_\ell^\eta(\tau)dx, \tag{17}$$

where

$$F_\ell^\eta(\tau) := \min_{0\le\theta\le1} \left\{F^\eta(\tau,\theta)+\ell\theta\right\}, \tag{18}$$

and $F^\eta(\tau,\theta)$ is defined as the so-called optimal lower bound on the effective complementary energy. More precisely, we introduce the subset G_θ^η of all possible anisotropic Hooke's laws of composite materials obtained by mixing A and η in proportions θ and $1-\theta$ (see Section 4 for details). Then

$$F^\eta(\tau,\theta) := \min_{A^*\in G_\theta^\eta} {A^*}^{-1}\tau\cdot\tau. \tag{19}$$

Finally in a third step, the weak material η is allowed to tend to zero. As η decreases to zero, we define the monotone limit

$$F(\tau,\theta) := \lim_{\eta\searrow0} F^\eta(\tau,\theta). \tag{20}$$

Similarly, we define the monotone limit

$$F_\ell(\tau) := \lim_{\eta\searrow0} F_\ell^\eta(\tau) = \min_{0\le\theta\le1} \left\{F(\tau,\theta)+\ell\theta\right\}. \tag{21}$$

The function F_ℓ turns out to be continuous in τ, but not convex. We shall prove in Section 3 that the relaxation of the optimization problem (8) is precisely

$$I(\ell) = I^*(\ell) := \min_{\tau\in\Sigma(\Omega)} \int_\Omega F_\ell(\tau)dx. \tag{22}$$

In [6] a proof of (22) is proposed in a 2-D setting at the expense of a non-trivial homogenization result pertaining to composite material obtained by rank-2 layering of the original material with void. Our purpose is to give a proof of the relaxation result which is valid for any spatial dimension as well as for any number of loading configurations.

Remark 2.3 *We have not said much so far about the function $F(\tau,\theta)$ defined as a monotone limit by (20). Loosely speaking, it is the optimal lower bound on the complementary energy for a perforated composite material obtained by mixing the material A with holes in proportions θ and $1-\theta$. Its properties will be examined in greater details in Section 4 below (see Corollary 4.4). Let us simply point out at this time the properties of F that will be of use in Section 3. The function $F(\tau,\theta)$ is given by the following formula*

$$F(\tau,\theta) = A^{-1}\tau\cdot\tau + \frac{1-\theta}{\theta}g^*(\tau), \tag{23}$$

where $g^*(\tau)$ is a continuous and convex function of τ only, homogeneous of degree 2, and strictly positive for any $\tau\neq0$. Therefore, F is continuous in (τ,θ) with values in

$I\!R^+ \cup \{+\infty\}$ *and strictly convex separately in* τ *and in* θ*. For any* $\tau \in I\!R_s^{N^2}$*, there exists a unique minimizer* θ *in (21) given by*

$$\theta = \min\left\{1, \sqrt{\frac{g^*(\tau)}{\ell}}\right\}. \tag{24}$$

Consequently, for any minimizer τ_ℓ *of the relaxed formulation (22), we associate through (24) a unique density function* θ_ℓ *that we call a relaxed, or generalized, optimal shape.*

Remark 2.4 *In the case of p different loadings, rewriting the optimization problem (9) in terms of stresses yields*

$$I_p(\ell) = \inf_{\{\tau_i\}\in\Sigma^p(\Omega)} \int_\Omega f_\ell^p\left(\{\tau_i\}\right) dx, \tag{25}$$

where

$$\Sigma^p(\Omega) := \left\{ \{\tau_i\}_{1\le i\le p} \in L^2(\Omega; I\!R_s^{N^2})^p \;\mid\; div\ \tau_i = 0 \text{ in } \Omega;\;\; \tau_i \cdot n = f_i \text{ on } \partial\Omega \right\},$$

and

$$f_\ell^p\left(\{\tau_i\}\right) := \begin{cases} 0 & \text{if all } \tau_i = 0, \\ \sum_{i=1}^p A^{-1}\tau_i\cdot\tau_i + \ell & \text{if at least one } \tau_i \neq 0. \end{cases} \tag{26}$$

Then, as in the case of a single load, we introduce a weak material η *and approximate* f_ℓ^p *defined in (26) by*

$$f_\ell^{p,\eta}\left(\{\tau_i\}\right) := \min\left\{ \sum_{i=1}^p A^{-1}\tau_i\cdot\tau_i + \ell, \sum_{i=1}^p \eta^{-1}\tau_i\cdot\tau_i \right\}.$$

Once again, as η *tends to zero, the sequence of functions* $f_\ell^{p,\eta}$ *monotonically converges to* f_ℓ^p*. The relaxation of the functional* $I_p(\ell,\eta)$*, with integrand* $f_\ell^{p,\eta}$*, is also classical [5], [6], and the result is similar to the single load case, namely*

$$I_p(\ell,\eta) = I_p^*(\ell,\eta) := \min_{\{\tau_i\}\in\Sigma^p(\Omega)} \int_\Omega F_\ell^{p,\eta}\left(\{\tau_i\}\right) dx,$$

where

$$F_\ell^{p,\eta}\left(\{\tau_i\}\right) := \min_{0\le\theta\le1}\left\{F^{p,\eta}\left(\{\tau_i\},\theta\right) + \ell\theta\right\}, \tag{27}$$

and $F^{p,\eta}$ *is defined as the so-called optimal lower bound on the sum of p effective complementary energies*

$$F^{p,\eta}\left(\{\tau_i\},\theta\right) := \min_{A^*\in G_\theta^\eta} \sum_{i=1}^p {A^*}^{-1}\tau_i\cdot\tau_i. \tag{28}$$

Then, as before, we define F^p *as the monotone limit of* $F^{p,\eta}$ *when* η *tends to zero. Introducing*

$$F_\ell^p\left(\{\tau_i\}\right) := \lim_{\eta\searrow0} F_\ell^{p,\eta}\left(\{\tau_i\}\right) = \min_{0\le\theta\le1}\left\{F^p\left(\{\tau_i\},\theta\right) + \ell\theta\right\}, \tag{29}$$

the relaxation of the original problem (25) is given by

$$I_p(\ell) = I_p^*(\ell) := \min_{\tau\in\Sigma^p(\Omega)} \int_\Omega F_\ell^p\left(\{\tau_i\}\right) dx. \tag{30}$$

The proof is very similar to that of the single load case (see Remark 3.7), because the functions $F^p(\{\tau_i\},\theta)$ and $F(\tau,\theta)$ enjoy similar properties. In particular, the analogue of (23) holds, i.e., *there exists a continuous, convex, positive, and homogeneous of degree 2 function $g_p^*(\{\tau_i\})$ such that (see Theorem 4.14)*

$$F^p(\{\tau_i\},\theta) = \sum_{i=1}^{p} {A^*}^{-1}\tau_i \cdot \tau_i + \frac{1-\theta}{\theta} g_p^*(\{\tau_i\}).$$

It implies that F^p is strictly convex in θ and that there exists a unique minimizer θ in (29) given by

$$\theta = \min\left\{1, \sqrt{\frac{g_p^*(\{\tau_i\})}{\ell}}\right\}. \tag{31}$$

Consequently, a unique optimal density is associated through (31) to any minimizer of the relaxed formulation (30).

We conclude this section with a brief recall of the notion of quasi-convexification of a real-valued functional W defined on $I\!R_s^{N^2}$. Let W be continuous and satisfy

$$0 \le W(\tau) \le \beta(1+|\tau|^2), \quad \tau \in I\!R_s^{N^2},$$

and define, for any bounded open domain Ω of $I\!R^N$,

$$\Sigma_0(\Omega) = \left\{\tau \in L^2(\Omega; I\!R_s^{N^2}) \;\mid\; div\ \tau = 0 \text{ in } \Omega\right\}.$$

The lower semi-continuous envelope in $\Sigma_0(\Omega)$ of

$$I(\tau) := \int_\Omega W(\tau)dx$$

for the sequential weak topology of $L^2(\Omega; I\!R_s^{N^2})$, *i.e.*, the functional

$$RI(\tau) := \inf_{\tau_n \in \Sigma_0(\Omega), \tau_n \rightharpoonup \tau \text{ weakly in } L^2(\Omega; I\!R_s^{N^2})} \liminf I(\tau_n)$$

is given by

$$RI(\tau) = \int_\Omega QW(\tau)dx. \tag{32}$$

The integrand QW is the quasi-convexification of W defined for every τ in $I\!R_s^{N^2}$ as

$$QW(\tau) := \inf_{s \in \Sigma_0(C), \int_C s(x)dx = \tau} \int_C W(s)dx,$$

where C is the unit cube of $I\!R^N$.

The integrand QW is a locally Lipschitz function as easily seen upon noting that QW is rank-$(N-1)$ convex and satisfies the same growth assumption as W (see e.g. [28]). In the present setting (18) may be restated as

$$F_\ell^\eta(\tau) = Qf_\ell^\eta(\tau), \tag{33}$$

with f_ℓ^η defined by (15). In other words F_ℓ^η is the quasi-convexification of f_ℓ^η.

Remark 2.5 *Until very recently, a proof of (32) was hard to locate in the literature because attention had been focussed primarily on functionals that depend on the gradient of a vector-valued field. In the latter setting the reader is referred to [15], Theorems 1.1 and 2.1 in Section 5, and to [1], Statement 3.7. A general study of quasiconvexity for functionals of vector fields that satisfy some first order differential constraints in the spirit of compensated compactness may now be found in [17] and it fills the existing gap.*

3 The relaxation process revisited.

This section revisits the derivation of the relaxed formulation for the unconstrained problem of least compliance and weight optimization introduced in Section 2. As already said, the relaxed formulation was already derived in [6], but a rigorous proof was only proposed in the two-dimensional setting. We saw in Section 2 that the shape optimization problem under consideration admits two equivalent formulations: that as a minimization over characteristic functions, and that as a problem of nonlinear elasticity in terms of stresses. We first give a complete relaxation theorem for the stress formulation, then deduce a partial relaxation result for the original formulation in terms of characteristic functions.

Theorem 3.1 *The stress formulation (12), (13) of the optimal shape problem admits (22) as a relaxed formulation. In other words, for any fixed value of the Lagrange multiplier $\ell \in [0; +\infty)$,*

1. *there exists at least one solution in $\Sigma(\Omega)$ of the relaxed minimization problem (22) and*
$$I(\ell) := \inf_{\tau \in \Sigma(\Omega)} \int_\Omega f_\ell(\tau)dx = I^*(\ell) := \min_{\tau \in \Sigma(\Omega)} \int_\Omega F_\ell(\tau)dx, \tag{34}$$
2. *up to a subsequence, any minimizing sequence of (12) converges weakly in $L^2(\Omega; I\!R_s^{N^2})$ to a minimizer of (22),*
3. *for any minimizer τ of (22) there exists a minimizing sequence of (12) which converges to τ weakly in $L^2(\Omega; I\!R_s^{N^2})$.*

The above result does not say anything about the link between the minimizing sequences of characteristic functions and the optimal densities in the relaxed formulation. Let us firstly recall that the integrand in the relaxed formulation is given by

$$F_\ell(\tau) = F(\tau, \theta_\tau) + \ell\theta_\tau, \tag{35}$$

where, by virtue of Remark 2.3, the volume fraction θ_τ is uniquely and unambiguously determined, once τ is known. Such a density function defines a so-called relaxed, or generalized, shape. It remains to understand in which sense the minimizing sequences of characteristic functions are related to this (possibly non-unique) optimal density. This is the object of the following

Proposition 3.2 *For any fixed Lagrange multiplier $\ell \in [0; +\infty)$, there exists at least one relaxed optimal shape,* i.e., *a density θ_ℓ. Furthermore, for any minimizing sequence of characteristic functions $\chi_n \in L^\infty(\Omega; \{0,1\})$, there exists a subsequence and a limit density θ_ℓ such that this subsequence converges to θ_ℓ weak-$_*$ in $L^\infty(\Omega; \{0,1\})$ and θ_ℓ is a relaxed optimal shape,* i.e., *it is associated through (35) to a minimizer of the relaxed formulation (22).*

Remark 3.3 *Proposition 3.2 is a weak version of the desired result of relaxation. In truth we aimed at proving that any minimizer τ_ℓ of (22) and its associated density θ_ℓ are attained as weak limits of a sequence $(\tau_n, \chi_n) \in \Sigma(\Omega) \times L^\infty(\Omega; \{0,1\})$ satisfying (11),* i.e., *such that*

$$\begin{cases} \tau_n(x) = 0 \text{ iff } \chi_n(x) = 0 & a.e. \text{ in } \Omega, \\ \chi_n \rightharpoonup \theta_\ell & weak\text{-}_* \text{ in } L^\infty(\Omega; [0,1]), \\ \tau_n \rightharpoonup \tau_\ell & weakly \text{ in } L^2(\Omega; I\!R_s^{N^2}), \\ \displaystyle\int_\Omega A^{-1}\tau_n \cdot \tau_n dx \to \int_\Omega F(\tau_\ell, \theta_\ell) dx, & \end{cases} \tag{36}$$

and conversely that any minimizing sequence (τ_n, χ_n) of the original problem converges, up to a subsequence, to a limit (τ_ℓ, θ_ℓ) which minimizes the relaxed problem. Unfortunately, we are unable to keep track of the fields τ_n which are such that (τ_n, χ_n) "minimizes" (10). In particular we do not know how to relate the weak limit of τ_n to τ_ℓ.

Remark 3.4 *Since by Theorem 3.1 we have proved the existence of at least one minimizer τ for the relaxed formulation $I^*(\ell)$, and consequently of one associated optimal density θ, the next obvious question concerns the uniqueness of such minimizers. Remark first that uniqueness in τ implies uniqueness in θ, but the converse is a priori false (there may well be different minimum stress fields τ that yield the same optimal density θ). It turns out that there is, in general, no uniqueness of either the minimizer τ or the optimal density θ. In Proposition 4.13 we shall construct a specific example for which there is an infinite number of minimizers τ and optimal densities θ. Furthermore, these optimal densities are actually "classical" shapes, namely they take only the values* 0 *or* 1 *(*i.e., *they are characteristic functions). Let us briefly describe this example: take any smooth domain Ω and impose a constant hydrostatic load on its boundary. In other words, select a boundary condition $\sigma.n = \sigma_0.n$ on $\partial\Omega$, where σ_0 is hydrostatic,* i.e., *$\sigma_0 = p_0 I_2$, with p_0 a constant scalar (the pressure) and I_2 the identity matrix. In this case, it is well known that the "concentric spheres construction" of Hashin achieves optimality in the original optimization problem $I(\ell)$, and thus in its relaxed formulation $I^*(\ell)$ (see (34)). There exist an infinite number of such constructions, depending on the chosen Vitali covering of Ω by spheres. Further details are given in Proposition 4.13.*

This example is also interesting since it shows that "classical" optimal shapes may exists for the original problem $I(\ell)$. However, even in this "lucky" case, the relaxed formulation $I^*(\ell)$ is not useless from a numerical standpoint. Indeed, it is a desperate task to try to compute numerically an optimal design built from an assemblage of concentric spheres which usually features an infinite number of holes (or connected components of the boundary). Furthermore, the mesh size would act as a threshold for the size of the smallest spheres, thus preventing optimality in a discrete computation.

Remark 3.5 *Coming back to the constrained formulation (5) of the optimal shape design problem, a complete relaxation process would amount to a rigorous proof of the existence, for each* $0 < \Theta < |\Omega|$*, of a multiplier* ℓ *for which the relaxed problem*

$$I^*(\ell) = \min_{\tau \in \Sigma(\Omega)} \int_\Omega F_\ell(\tau) dx$$

admits a solution $\tau_\ell \in \Sigma(\Omega)$ *such that the total volume fraction of material coincides with* Θ*,* i.e.

$$\Theta = \int_\Omega \theta_\ell dx.$$

We are unable to prove the existence of such a value of ℓ *; indeed, we are in want of a proof that the function*

$$\Theta(\ell) := \int_\Omega \theta_\ell dx$$

is continuous in ℓ*. In fact,* $\Theta(\ell)$ *may well be a multi-valued function since the optimal density* θ_ℓ *is not necessarily unique. We will merely establish in Lemma 3.6 below that it is a decreasing function of* ℓ *and that it goes to zero as* ℓ *goes to infinity, provided that the surface loadings are "smooth enough". The continuity of* $\Theta(\ell)$ *is at present an open question.*

Proof of Theorem 3.1: It is a straightforward consequence of the fact that F_ℓ defined in (21) is the quasi-convexification of f_ℓ defined in (14) in the sense of (32). We prove this statement.

Since f_ℓ^η monotonically increases to f_ℓ as η tends to zero, we have

$$F_\ell^\eta(\tau) = Qf_\ell^\eta(\tau) \le Qf_\ell(\tau), \quad \tau \in I\!R_s^{N^2}.$$

But F_ℓ^η monotonically increases to F_ℓ as η tends to zero. Thus

$$F_\ell(\tau) \le Qf_\ell(\tau), \quad \tau \in I\!R_s^{N^2}.$$

The integrand Qf_ℓ is quasi-convex and it has at most quadratic growth. Thus it is easily seen in the spirit of Part 3 of the proof of Theorem 1.1 in Section 4.1 of [15] that Qf_ℓ is rank-$(N-1)$ convex, hence continuous. Define

$$g_\ell^\eta(\tau) := \min\left\{f_\ell^\eta(\tau), Qf_\ell(\tau)\right\}.$$

It is a monotone sequence of continuous functions that converges, as η tends to zero, to a continuous function, namely Qf_ℓ, and Dini's theorem implies the uniform convergence of g_ℓ^η to Qf_ℓ over any compact subset of $I\!R_s^{N^2}$. Further

$$Qg_\ell^\eta(\tau) \le Qf_\ell^\eta(\tau) = F_\ell^\eta(\tau),$$

because $g_\ell^\eta \le f_\ell^\eta$. Thus

$$\lim_{\eta \searrow 0} Qg_\ell^\eta(\tau) \le F_\ell(\tau) \le Qf_\ell(\tau).$$

We now prove that

$$Qf_\ell(\tau) \le \lim_{\eta \searrow 0} Qg_\ell^\eta(\tau), \tag{37}$$

which, in view of the previous inequality, establishes that F_ℓ is the quasi-convexification of f_ℓ, *i.e.*, $F_\ell = Qf_\ell$. For any τ in $I\!R_s^{N^2}$ and any positive fourth order tensor η, there exists a test function s_η in $\Sigma_0(C)$ with $\int_C s_\eta(x)dx = \tau$ such that

$$Qg_\ell^\eta(\tau) \geq \int_C g_\ell^\eta(s_\eta)dx - |\eta|$$

$$\geq \int_C Qf_\ell(s_\eta)dx - |\eta| - \int_C |g_\ell^\eta - Qf_\ell|(s_\eta)dx.$$

But $g_\ell^\eta(\tau) = Qf_\ell(\tau)$ as soon as $|\tau|$ is large enough (say $|\tau| \geq M$ where M is independent of η). Thus, for any positive ϵ,

$$\int_C |g_\ell^\eta - Qf_\ell|(s_\eta)dx = \int_{C\cap\{|s_\eta(x)|\leq M\}} |g_\ell^\eta - Qf_\ell|(s_\eta)dx \leq \epsilon,$$

whenever η is small enough, because of the uniform character of the convergence of g_ℓ^η to Qf_ℓ over the compact set $\{s \in I\!R_s^{N^2} |s| \leq M\}$. Thus, for any positive ϵ and for η small enough, we have

$$Qg_\ell^\eta(\tau) \geq \int_C Qf_\ell(s_\eta)dx - |\eta| - \epsilon \geq Qf_\ell(\tau) - |\eta| - \epsilon,$$

by virtue of the quasi-convex character of Qf_ℓ. This proves (37). To complete the proof of Theorem 3.1 it remains to check that F_ℓ is coercive, and is sequentially weakly lower semi-continuous over $\Sigma(\Omega)$. This is obvious since

$$F_\ell(\tau) \geq A^{-1}\tau\cdot\tau, \quad \tau \in I\!R_s^{N^2},$$

and $\int_\Omega F_\ell^\eta dx$ is sequentially weakly lower semi-continuous, a property which carries over as η tends to zero. Thus the minimization problem

$$\min_{\tau\in\Sigma(\Omega)} \int_\Omega F_\ell(\tau)dx$$

admits a solution τ_ℓ in $\Sigma(\Omega)$ and (34) is indeed a relaxed formulation of (12).

Proof of Proposition 3.2: Let us consider a minimizing sequence $\chi_n \in L^\infty(\Omega;\{0,1\})$ of the original problem $I(\ell)$ defined by (5) and (8) which converges weak-$_*$ to some limit θ_ℓ in $L^\infty(\Omega;[0,1])$. For any admissible test function $\tau \in \Sigma(\chi_n)$, we have

$$\int_\Omega A^{-1}\tau\cdot\tau dx = \int_\Omega \left(\chi_n A^{-1} + (1-\chi_n)\eta^{-1}\right)\tau\cdot\tau dx \geq \min_{\sigma\in\Sigma(\Omega)} \int_\Omega \left(\chi_n A^{-1} + (1-\chi_n)\eta^{-1}\right)\sigma\cdot\sigma dx. \tag{38}$$

As soon as η is positive, the minimum in the right hand side of (38) is attained by a unique τ_n^η. Thus, minimizing in τ, and recalling that χ_n is a minimizing sequence of $I(\ell)$, yield

$$I(\ell) \geq \limsup_n \left\{\int_\Omega \left(\chi_n A^{-1} + (1-\chi_n)\eta^{-1}\right)\tau_n^\eta\cdot\tau_n^\eta dx + \ell\int_\Omega \chi_n dx\right\}. \tag{39}$$

According to the theory of H-convergence (see e.g. [32], [37]), a subsequence of $A_\eta^n := \chi_n A + (1-\chi_n)\eta$ H-converges to a tensor A_η^* as n goes to infinity. Thus, the corresponding τ_n^η weakly converges in $L^2(\Omega; I\!R_s^{N^2})$ to an element $\tau^\eta \in L^2(\Omega; I\!R_s^{N^2})$, and, for that subsequence,

$$\int_\Omega \left(\chi_n A^{-1} + (1-\chi_n)\eta^{-1}\right)\tau_n^\eta\cdot\tau_n^\eta dx \to \int_\Omega (A_\eta^*)^{-1}\tau^\eta\cdot\tau^\eta dx. \tag{40}$$

Consequently (39) and (40) imply that

$$I(\ell) \geq \int_\Omega (A_\eta^*)^{-1}\tau^\eta \cdot \tau^\eta dx + \ell \int_\Omega \theta_\ell dx. \tag{41}$$

Since $I(\ell)$ is finite (F_ℓ has quadratic growth at infinity), the sequence τ^η is bounded in $L^2(\Omega; I\!R_s^{N^2})$ independently of η. A subsequence, still indexed by η, is such that, as η goes to zero, τ^η converges weakly to some τ_ℓ in $L^2(\Omega; I\!R_s^{N^2})$. Furthermore, since

$$\|A_\eta^n - A_{\eta'}^n\|_{L^\infty(\Omega)} \leq |\eta - \eta'|,$$

the same holds true for the H-limits as n tends to infinity, *i.e.*,

$$\|A_\eta^* - A_{\eta'}^*\|_{L^\infty(\Omega)} \leq |\eta - \eta'|.$$

Hence A_η^* converges uniformly to A^* as η goes to zero. The convex character of the mapping

$$(A, \tau) \to A^{-1}\tau \cdot \tau$$

yields

$$\liminf_\eta \int_\Omega (A_\eta^*)^{-1}\tau^\eta \cdot \tau^\eta dx \geq \int_\Omega (A^*)^{-1}\tau_\ell \cdot \tau_\ell dx,$$

for which it is deduced, upon recalling (41), that

$$I(\ell) \geq \int_\Omega (A^*)^{-1}\tau_\ell \cdot \tau_\ell dx + \ell \int_\Omega \theta_\ell dx. \tag{42}$$

Introduce the subset $\mathcal{G}_\theta^\eta$ of $L^\infty\left(\Omega; \mathcal{L}_s(I\!R_s^{N^2})\right)$ defined as

$$\mathcal{G}_\theta^\eta := \{H\text{-limits of } A^n = \chi_n A + (1-\chi_n)\eta \ \mid\ \chi_n \rightharpoonup \theta\}.$$

According to [16], for all $0 \leq \theta \leq 1$, there exists a fixed subset G_θ^η of $\mathcal{L}_s(I\!R_s^{N^2})$ such that

$$\mathcal{G}_\theta^\eta = \{A(x) \text{ measurable } \mid A(x) \in G_{\theta(x)}^\eta \text{ a.e. in } \Omega\}.$$

Consequently $A^*(x) \in G_{\theta_\ell(x)}^0$ a.e. in Ω, where G_θ^0 is the algebraic limit of G_θ^η as η goes to zero.

Recall that $F^\eta(\tau, \theta)$ is defined as (see (19))

$$F^\eta(\tau, \theta) := \min_{B \in G_\theta^\eta} B^{-1}\tau \cdot \tau.$$

Therefore its monotone limit $F(\tau, \theta)$, as η tends to zero, is given by

$$F(\tau, \theta) = \inf_{B \in G_\theta^0} B^{-1}\tau \cdot \tau. \tag{43}$$

Since $A^*(x) \in G_{\theta_\ell(x)}^0$ a.e. in Ω, we deduce from (42) and (43) that

$$\begin{aligned} I(\ell) &\geq \int_\Omega F(\tau_\ell, \theta_\ell) dx + \ell \int_\Omega \theta_\ell dx \\ &\geq \int_\Omega \min_{0 \leq \theta \leq 1} \left(F(\tau_\ell, \theta) + \ell\theta\right) dx \\ &\geq \int_\Omega F_\ell(\tau_\ell) dx. \end{aligned}$$

By Theorem 3.1 τ_ℓ is a minimizer of $I^*(\ell)$, and the above inequalities become equalities. Furthermore, by virtue of the strict convexity in θ of $F(\tau,\theta)$, θ_ℓ is the unique density associated to τ_ℓ through minimization in θ, a.e. in Ω. This concludes the proof of Proposition 3.2.

We next prove the result announced in Remark 3.5.

Lemma 3.6 *Define the multi-valued function*

$$\Theta(\ell) := \int_\Omega \theta_\ell dx,$$

where θ_ℓ is the optimal density associated to any (possibly non-unique) minimizer τ_ℓ of the relaxed problem $I^*(\ell)$. It is a decreasing function of ℓ. Furthermore, $\Theta(\ell)$ goes to zero as ℓ goes to infinity, provided that the surface load f is such that there exists at least one admissible test field $\sigma \in \Sigma(\Omega)$ which is uniformly bounded in Ω.

Proof: Assume that $\ell > \ell' \geq 0$, and take any minimizer τ_ℓ (resp. $\tau_{\ell'}$) of $I^*(\ell)$ (resp. $I^*(\ell')$) and its associated optimal density θ_ℓ (resp. $\theta_{\ell'}$). We start from

$$I^*(\ell') = \int_\Omega F(\tau_{\ell'},\theta_{\ell'})dx + \ell'\Theta(\ell') \leq \int_\Omega F(\tau_\ell,\theta_\ell)dx + \ell'\Theta(\ell),$$

which is equivalent to

$$\int_\Omega F(\tau_{\ell'},\theta_{\ell'})dx + \ell\Theta(\ell') \leq \int_\Omega F(\tau_\ell,\theta_\ell)dx + \ell\Theta(\ell) + (\ell-\ell')\left(\Theta(\ell')-\Theta(\ell)\right). \qquad (44)$$

Since the sum of the two first terms in the right hand side of (44) is precisely $I^*(\ell)$, the minimum value of

$$\int_\Omega F(\tau,\theta)dx + \ell\int_\Omega \theta dx,$$

the last term of (44) must be positive. This yields

$$\Theta(\ell) \leq \Theta(\ell').$$

Now, assume that the surface load f is such that there exists at least one admissible test field $\sigma_0 \in \Sigma(\Omega)$ which is uniformly bounded in Ω. Then, the density θ_0, associated through formula (24), satisfies

$$\theta_0 \leq \frac{C}{\sqrt{\ell}},$$

for ℓ large enough. Consequently,

$$F_\ell(\sigma_0) \leq C(1+\sqrt{\ell}) \text{ a.e. in } \Omega.$$

Thus any minimizing pair (τ_ℓ,θ_ℓ) satisfies

$$I^*(\ell) = \int_\Omega F(\tau_\ell,\theta_\ell)dx + \ell\Theta(\ell) \leq C(1+\sqrt{\ell}),$$

which proves that $\Theta(\ell)$ goes to zero when ℓ goes to infinity at least as fast as $\ell^{-1/2}$.

Remark 3.7 *The relaxation results, Theorem 3.1 and Proposition 3.2, still hold true for a problem with multiple loads, as introduced in Remarks 2.2 and 2.4. Indeed, it is not difficult to check the main ingredient of the proof of Theorem 3.1, namely that the integrand $F_\ell^p(\{\tau_i\})$ of the relaxed formulation (30) is the quasi-convexification of the integrand $f_\ell^p(\{\tau_i\})$ of the original formulation (25). Similarly, the proof of Proposition 3.2 goes through in the multiple loads case.*

Remark 3.8 *The proofs of Theorem 3.1 and Proposition 3.2 rest on the choice of the compliance (or sum of compliances in the multiple loads case) as the objective function because we use various properties of the relaxed functional (such as the strict convexity of $F(\tau,\theta)$ with respect to θ) specific to the case under investigation. When other objective functionals, such as the maximum value for the stress or the displacement, are considered, the results of Theorem 3.1 and Proposition 3.2 are not obvious. Furthermore the relaxation process involves a minimization over all fourth order tensor A^*_η in the so-called G-closure set G^η_θ,* i.e., *in the set of effective Hooke's law of composite materials obtained by mixing A and η in proportions θ and $(1-\theta)$. Unfortunately, an algebraic characterization of the set G^η_θ (and of its limit when η tends to zero) is lacking. Therefore, the relaxed formulation for a general objective functional is useless because of the absence of a characterization of the precise class of generalized admissible designs! In a compliance optimization problem, the relaxed formulation can be further simplified: as a consequence of the results of Section 4 below , the set G^η_θ of admissible designs can be restricted to the set of sequentially laminated composites which is better understood. In this case, the relaxed formulation is explicit and becomes amenable to numerical computations (see Section 5 to 8 below).*

4 Explicit formula for the relaxed energy.

This section is devoted to the computation of the integrand

$$F_\ell(\tau) = \min_{0\le\theta\le 1} \left(F(\tau,\theta) + \ell\theta\right)$$

of the relaxed functional $I^*(\ell)$. This computation is as explicit as possible since it is at the root of the numerical algorithm proposed in Section 5 below. It begins with a review of known results that permit to view $F(\tau,\theta)$ as the effective energy, at the stress τ, of the most rigid composite of density θ, which turns out to be a sequential laminate of rank N.

It is a known result (see e.g. Section 3 in [6]) on the homogenization of mixtures of two materials A and η, where η is the weak material that occupies the holes, A and η being positive definite, symmetric, fourth order tensors, that

$$F^\eta(\tau,\theta) = \min_{A^*\in G^\eta_\theta} {A^*}^{-1}\tau\cdot\tau, \tag{45}$$

where G^η_θ is the set of all possible anisotropic Hooke's laws of composite materials obtained by mixing A and η in volume fractions θ and $1-\theta$. Formula (45) is called an optimal lower bound on the effective complementary energy.

To compute the minimum in the right hand side of (45), it would be helpful to have an algebraic definition of the G-closure set G^η_θ. Unfortunately, the theory is helpless in the matter. For the special case of elastic energies as in (45), however, it is proved in [7] that the minimum is actually attained within a well-known subset of G_θ^η, that of finite rank sequential laminates, denoted by L_θ^η.

Let us first recall appropriate layering formulae [18]. Throughout this section, we assume that the material A is isotropic; for any symmetric matrix ξ,

$$A\xi = 2\mu\xi + \lambda(tr\xi)I_2,$$

where I_2 is the identity matrix, and (μ, λ) are the Lamé coefficients of the material. The shear modulus μ is always positive so as to ensure coerciveness of the Hooke's law; the bulk modulus $\kappa = \lambda + 2\mu/N$ is also required to be positive if strong ellipticity is to hold. It turns out that most materials have a non negative Poisson ratio, *i.e.*, that $\lambda \geq 0$. Since this last hypothesis greatly simplifies the computations (at least in the three dimensional setting), we shall assume henceforth that

$$\mu > 0, \quad \lambda \geq 0.$$

Proposition 4.1 *Let A^* be a rank-p sequential laminate of material A around a core of material η, in proportion θ and $(1-\theta)$ respectively, with lamination directions $(e_i)_{1\leq i\leq p}$ and lamination parameters $(m_i)_{1\leq i\leq p}$ satisfying $0 \leq m_i \leq 1$ and $\sum_{i=1}^p m_i = 1$ (these parameters are related to the volume fractions of material A at each step of the lamination process). Then*

$$(1-\theta)\left(A^{*^{-1}} - A^{-1}\right)^{-1} = \left(\eta^{-1} - A^{-1}\right)^{-1} + \theta \sum_{i=1}^{p} m_i f_A^c(e_i) \tag{46}$$

where $f_A^c(e_i)$ is a fourth order tensor defined, for any symmetric matrix ξ, by the quadratic form

$$f_A^c(e_i)\xi \cdot \xi = A\xi \cdot \xi - \frac{1}{\mu}|A\xi e_i|^2 + \frac{\mu + \lambda}{\mu(2\mu + \lambda)}((A\xi)e_i \cdot e_i)^2,$$

where (μ, λ) are the Lamé coefficients of A.

A proof of the lamination formula (46) would parallel that of Proposition 4.2 in [18] using complementary energy instead of primal energy. Note that $f_A^c(e_i)$ is a degenerate Hooke's law in the sense that it is a non negative, semi-definite, fourth order tensor.

Theorem 4.2 *Whenever η is a weaker material than A (i.e., $A - \eta$ is a non negative fourth order tensor), the optimal bound (45) is given by*

$$F^\eta(\tau, \theta) = \min_{A^* \in L_\theta^\eta} A^{*^{-1}}\tau \cdot \tau, \tag{47}$$

where L_θ^η is the set of all effective Hooke's law of finite rank sequential laminates defined through (46). Furthermore, optimality in the right hand side of (47) is achieved by a rank-N sequential laminate (in space dimension N) with lamination directions coïnciding with the eigendirections of the symmetric matrix τ.

As already mentioned, the first part of Theorem 4.2 may be found [7], while the second part is to be found in [5]. For details, the reader is referred to e.g. formulae (6.11), (6.18), and (7.6) and Remark 3.7 in [5].

Remark 4.3 *In Theorem 4.2 the optimal microstructure is not always unique. In the first place, the optimal sequential laminate may not be uniquely defined. For example, in the case of an hydrostatic stress (*i.e., *τ proportional to the identity I_2), any orthonormal basis of $\mathbb{R}^N$ is a set of eigenvectors of τ and thus a set of lamination directions. It can be checked not to lead to the same homogenized Hooke's law. There is another type of non-uniqueness: sequential laminates are not the only known class of optimal microstructures (although probably the easiest to work with). For example, the so-called concentric spheres construction [22] (generalized in [38] to confocal ellipsoids), or the periodic arrangement of adequately shaped inclusions in [39] (see also [21]) are also optimal in specific situations.*

In truth, we are interested in $F(\tau, \theta)$, *i.e.*, in the limit of (47) as η tends to zero, but it is not difficult to pass to the limit in the lamination formula (46) and, thus, to define a limit set L_θ^0. Furthermore, when $\eta = 0$ the degenerate lamination formula can be rewritten as

$$A^{*-1} = A^{-1} + \frac{1-\theta}{\theta} \left(\sum_{i=1}^{p} m_i f_A^c(e_i) \right)^{-1}, \tag{48}$$

at least when restricted to the subspace of symmetric matrices where the sum of degenerate Hooke's law $\sum_{i=1}^{p} m_i f_A^c(e_i)$ is invertible. Therefore, as η goes to zero, Theorem 4.2 yields the following corollary.

Corollary 4.4 *The function $F(\tau, \theta)$, defined as the monotone limit of $F^\eta(\tau, \theta)$ when η tends to zero, is given by*

$$F(\tau, \theta) = \min_{A^* \in L_\theta^0} A^{*-1} \tau \cdot \tau, \tag{49}$$

where L_θ^0 is the set of all tensors A^* defined by formula (48).

Furthermore, since optimality is achieved for a rank-N sequential laminate with lamination directions given by the eigendirections of τ, (49) becomes

$$F(\tau, \theta) = A^{-1}\tau \cdot \tau + \frac{1-\theta}{\theta} g^*(\tau), \tag{50}$$

where $g^*(\tau)$ is a continuous and convex function of τ, homogeneous of degree 2, strictly positive for $\tau \neq 0$, defined by

$$g^*(\tau) = \min_{m_i \geq 0, \sum_{i=1}^{N} m_i = 1} \left(\sum_{i=1}^{N} m_i f_A^c(e_i) \right)^{-1} \tau \cdot \tau, \tag{51}$$

where the vectors $(e_i)_{1 \leq i \leq N}$ are the normalized eigenvectors of τ.

The only non-obvious statement of Corollary 4.4 is that concerning the properties of g^*. To check them, one can use the Legendre transform to rewrite

$$\left(\sum_{i=1}^{N} m_i f_A^c(e_i) \right)^{-1} \tau \cdot \tau = \max_{\xi} \left\{ 2\xi \cdot \tau - \sum_{i=1}^{N} m_i f_A^c(e_i) \xi \cdot \xi \right\}.$$

Then, g^* is easily seen to be defined as a saddle point: the min and the max can be exchanged, which yields the desired properties.

In view of Corollary 4.4 the computation of $F(\tau,\theta)$ amounts to a simple optimization of the lamination parameters m_i of a rank-N sequential laminate, while the lamination directions e_i are kept fixed and equal to the eigendirections of τ. However, the lamination formula (48) yields ${A^*}^{-1}$ at the price of a non trivial inversion of a sum of degenerate Hooke's law. Inverting this sum in full generality is a difficult task. In any case we need only address the class of so-called *orthogonal* rank-N sequential laminates which, by definition, admit an orthonormal basis of $I\!R^N$ as lamination directions $(e_i)_{1\leq i\leq N}$. We now recall a result concerning Hooke's laws for orthogonal rank-N sequential laminates [3].

Lemma 4.5 *The inverse Hooke's law* ${A^*}^{-1}$ *of an orthogonal rank-N sequential laminate is given by the following quadratic form*

$$ {A^*}^{-1}\tau\cdot\tau = A^{-1}\tau\cdot\tau + \frac{1-\theta}{2\mu\theta}G(\alpha_i,\tau) \tag{52} $$

with

$$ \begin{aligned} G(\alpha_i,\tau) &= \sum_{i,j=1,i\neq j}^{N} \frac{\tau_{ij}^2}{(1-m_i-m_j)} + \sum_{i=1}^{N}\alpha_i\tau_{ii}^2 \\ &\quad -\frac{\lambda}{2\mu+N\lambda}\left(\sum_{i=1}^{N}\tau_{ii}\right)^2 + \frac{\lambda}{2\mu+N\lambda}\frac{\left(\sum_{i=1}^{N}(\alpha_i-1)\tau_{ii}\right)^2}{(1-\frac{\lambda}{2\mu+N\lambda}\sum_{i=1}^{N}\alpha_i)}, \end{aligned} $$

where τ_{ij} denotes the entries of a symmetric matrix τ in the orthonormal basis of lamination directions, and the parameters $(\alpha_i)_{1\leq i\leq N}$ are defined by

$$ \alpha_i = \left(1-\frac{2\mu m_i}{2\mu+\lambda}\right)^{-1}. $$

Remark 4.6 *The quadratic form (52) defines a coercive Hooke's law A^* in dimension $N\geq 3$ as soon as none of the parameters m_i are zero, that is whenever all lamination directions have been put to use. (Indeed, $m_i>0$ for $1\leq i\leq N$ implies that $1-m_i-m_j>0$ for $1\leq i,j\leq N$ and $i\neq j$.) Thus, in three dimensions, an orthogonal rank-3 laminate is a realistic composite material. On the contrary, in two dimensions, we always have $1-m_i-m_j=0$! Thus, formula (52) only holds for stresses τ which are diagonal in the basis of lamination directions (*i.e.*, such that $\tau_{ij}=0$). In other words, in 2-D, an orthogonal rank-2 laminate cannot support a stress whose eigendirections are not aligned with the lamination directions. This fact has been previously emphasized by several authors [4], [24], and it bears important consequences for the numerical algorithm to be discussed in Section 5. Remark also that an orthogonal rank-N laminate is not isotropic even if all lamination parameters m_i are set equal to $1/N$. It is shown in [19] that three laminations in 2-D, and six in 3-D, are required to obtain an isotropic effective Hooke's law.*

Thanks to the above lemma we now optimize in m_i the right hand side of (51) and compute the precise value of g^*,

$$g^*(\tau) = \frac{1}{2\mu} \min_{m_i \geq 0, \sum_{i=1}^N m_i = 1} G(\alpha_i, \tau).$$

In two dimensions, this computation has been performed in [6]; it yields the following

Proposition 4.7 *In two dimensions,*

$$g^*(\tau) = \frac{\lambda}{4\mu(\mu+\lambda)} \left(|\tau_1| + |\tau_2|\right)^2 \tag{53}$$

where τ_1 and τ_2 are the eigenvalues of the stress τ (a two by two symmetric matrix in 2-D). Furthermore, the associated optimal rank-2 sequential laminate is characterized by its parameters

$$m_1 = \frac{|\tau_2|}{|\tau_1| + |\tau_2|}, \quad m_2 = \frac{|\tau_1|}{|\tau_1| + |\tau_2|}. \tag{54}$$

In three dimensions, the computation is more involved (cf. [3] or [20]). It yields the following

Proposition 4.8 *In three dimensions, if $\tau_1 \leq \tau_2 \leq \tau_3$ are the eigenvalues of τ, then*

1. *in the case where $0 \leq \tau_1 \leq \tau_2 \leq \tau_3$*

$$g^*(\tau) = \frac{2\mu+\lambda}{4\mu(2\mu+3\lambda)} \left(\tau_1 + \tau_2 + \tau_3\right)^2 \;\; \textit{if } \tau_3 \leq \tau_1 + \tau_2 \tag{55}$$

$$g^*(\tau) = \frac{1}{2\mu}\left((\tau_1+\tau_2)^2 + \tau_3^2\right) - \frac{\lambda}{2\mu(2\mu+3\lambda)} \left(\tau_1 + \tau_2 + \tau_3\right)^2 \;\; \textit{if } \tau_3 \geq \tau_1 + \tau_2 \tag{56}$$

2. *in the case where $\tau_1 \leq 0 \leq \tau_2 \leq \tau_3$*

$$g^*(\tau) = \frac{2\mu+\lambda}{4\mu(2\mu+3\lambda)} \left(\tau_3 + \tau_2 - \frac{\mu+2\lambda}{\mu+\lambda}\tau_1\right)^2 \;\; \textit{if } \begin{cases} \tau_3 + \tau_2 \geq -\frac{\mu}{\mu+\lambda}\tau_1 \\ \tau_3 - \tau_2 \leq -\frac{\mu}{\mu+\lambda}\tau_1 \end{cases} \tag{57}$$

$$g^*(\tau) = \frac{1}{2\mu}\left((\tau_3+\tau_2)^2 + \tau_1^2\right) - \frac{\lambda}{2\mu(2\mu+3\lambda)} \left(\tau_1 + \tau_2 + \tau_3\right)^2 \;\; \textit{if } \tau_3 + \tau_2 \leq -\frac{\mu}{\mu+\lambda}\tau_1 \tag{58}$$

$$g^*(\tau) = \frac{1}{2\mu}\left(\tau_1^2 + \tau_2^2 + \tau_3^2\right) - \frac{2\mu}{2\mu(\mu+\lambda)}\tau_1\tau_2 - \frac{\lambda}{2\mu(2\mu+3\lambda)} \left(\tau_1 + \tau_2 + \tau_3\right)^2 \;\; \textit{if } \tau_3 - \tau_2 \geq -\frac{\mu}{\mu+\lambda}\tau_1 \tag{59}$$

3. *the remaining cases are obtained from (1) and (2) by symmetry, changing τ into $-\tau$.*

Furthermore, optimality in the regime (55) is achieved by a rank-3 sequential laminate with parameters

$$m_1 = \frac{\tau_3 + \tau_2 - \tau_1}{\tau_1 + \tau_2 + \tau_3}, \quad m_2 = \frac{\tau_1 - \tau_2 + \tau_3}{\tau_1 + \tau_2 + \tau_3}, \quad m_3 = \frac{\tau_1 + \tau_2 - \tau_3}{\tau_1 + \tau_2 + \tau_3}; \tag{60}$$

in the regime (56) it is achieved by a rank-2 sequential laminate with parameters

$$m_1 = \frac{\tau_2}{\tau_1 + \tau_2}, \quad m_2 = \frac{\tau_1}{\tau_1 + \tau_2}, \quad m_3 = 0; \tag{61}$$

in the regime (57) it is achieved by a rank-3 sequential laminate with parameters

$$m_1 = \frac{\tau_3 + \tau_2 + \dfrac{\mu}{\mu+\lambda}\tau_1}{\tau_3 + \tau_2 - \dfrac{\mu+2\lambda}{\mu+\lambda}\tau_1}, \quad m_2 = \frac{\mu+\lambda}{\mu} \frac{\tau_3 - \tau_2 - \dfrac{\mu}{\mu+\lambda}\tau_1}{\tau_3 + \tau_2 - \dfrac{\mu+2\lambda}{\mu+\lambda}\tau_1}, \tag{62}$$

$$m_3 = -\frac{\mu+\lambda}{\mu} \frac{\tau_3 - \tau_2 + \dfrac{\mu}{\mu+\lambda}\tau_1}{\tau_3 + \tau_2 - \dfrac{\mu+2\lambda}{\mu+\lambda}\tau_1}; \tag{63}$$

in the regime (58) it is achieved by a rank-2 sequential laminate with parameters

$$m_1 = 0, \quad m_2 = \frac{\tau_3}{\tau_2 + \tau_3}, \quad m_3 = \frac{\tau_2}{\tau_2 + \tau_3}, \tag{64}$$

in the regime (59) it is achieved by a rank-2 sequential laminate with parameters

$$m_1 = \frac{\tau_2}{\tau_2 - \tau_1}, \quad m_2 = \frac{-\tau_1}{\tau_2 - \tau_1}, \quad m_3 = 0. \tag{65}$$

When the material has zero Poisson's ratio the above result greatly simplifies; we state it for the reader's convenience.

Corollary 4.9 *In three dimensions, assume that the material A satisfies $\lambda = 0$. Then, under the non-restrictive ordering assumption, $|\tau_1| \le |\tau_2| \le |\tau_3|$,*

$$g^*(\tau) = \frac{1}{4\mu}\left(|\tau_1| + |\tau_2| + |\tau_3|\right)^2 \ \textit{if}\ |\tau_3| \le |\tau_1| + |\tau_2|, \tag{66}$$

and

$$g^*(\tau) = \frac{1}{2\mu}\left((|\tau_1| + |\tau_2|)^2 + |\tau_3|^2\right) \ \textit{if}\ |\tau_3| \ge |\tau_1| + |\tau_2|. \tag{67}$$

Furthermore, optimality in the first regime (66) is achieved by a rank-3 sequential laminate with parameters

$$m_1 = \frac{|\tau_3| + |\tau_2| - |\tau_1|}{|\tau_1| + |\tau_2| + |\tau_3|}, \quad m_2 = \frac{|\tau_1| - |\tau_2| + |\tau_3|}{|\tau_1| + |\tau_2| + |\tau_3|}, \quad m_3 = \frac{|\tau_1| + |\tau_2| - |\tau_3|}{|\tau_1| + |\tau_2| + |\tau_3|},$$

while optimality in the second regime (67) is achieved by a rank-2 sequential laminate with parameters

$$m_1 = \frac{|\tau_2|}{|\tau_1| + |\tau_2|}, \quad m_2 = \frac{|\tau_1|}{|\tau_1| + |\tau_2|}, \quad m_3 = 0.$$

The above results which yield an explicit formula for the function $g^*(\tau)$ are at the root of the numerical algorithm proposed in Section 5. To compute the integrand $F_\ell(\tau)$ of the relaxed functional $I^*(\ell)$, it simply remains to optimize with respect to θ, which yields

$$F_\ell(\tau) = \begin{cases} A^{-1}\tau\cdot\tau+\ell & \text{if } g^*(\tau)\geq\ell, \\ A^{-1}\tau\cdot\tau+2\sqrt{\ell g^*(\tau)}-g^*(\tau) & \text{if } g^*(\tau)<\ell. \end{cases} \tag{68}$$

The optimal density is given by

$$\theta = \min\left\{1, \sqrt{\frac{g^*(\tau)}{\ell}}\right\}. \tag{69}$$

Note that, by virtue of Corollary 4.4, $\theta = 0$ if and only if $\tau = 0$, which means that holes are created only where the stress vanishes.

A common feature of the above formulae is that they involve the eigenvalues of the stress τ. The optimal microstructure (namely the rank-N laminate) adapts itself to the stress that it should sustain, by aligning its lamination directions with the principal directions of the stress and adopting in each layer a volume fraction which is controlled by the values of the principal stresses. This correlation between microstructure and stress is a rigorous consequence of the homogenization theory and not a postulate. In particular in 2-D we recover the well-known principle of material economy in frame-structures due to Michell [29].

Remark 4.10 *In two dimensions, when the Lagrange multiplier ℓ goes to infinity, it is formally shown in [6] that the relaxed problem is asymptotically equivalent to the so-called* Michell trusses *problem*

$$\min_{\tau\in\Sigma(\Omega)} \int_\Omega (|\tau_1|+|\tau_2|)\,dx,$$

where τ_1, τ_2 are the eigenvalues of the stress τ. Note that this result is also immediately recovered from (53) and (68). There is a rich literature on this problem (see e.g. [34], [35]), and we refer the interested reader to Section 6 of [6] for a brief discussion of Michell trusses in our context. Note that this limiting case of the relaxed formulation may explain the success of our computations, and more precisely the fact that many of our optimal structures look like a network of trusses, or bars, in 2-D.

In 2-D only one type of optimal laminates, namely rank-2 laminates, are used (although they can degenerate to rank-1 when one of the eigenvalues vanishes). On the contrary, in 3-D there are two distinct regimes of optimal laminates: rank-3 or rank-2 (which in turn can degenerate to rank-1). This can be easily explained as follows. The conditions defining regimes (55) or (57), where a rank-3 laminate is optimal, imply that the three principal stresses are of the same order of magnitude. This means that the material can be optimally layered in the three principal directions, creating a microstructure made of plate-like holes in a matrix of material. On the other hand, the remaining regimes (56), (58), or (59), where a rank-2 laminate is optimal, correspond to a setting where one of the principal stresses is large compared to the other two. In this case, it is more economical not to layer in the direction of the largest principal stress, and simply to translate, in this direction, a planar optimal microstructure which allows the available material to sustain the largest stress in the direction of translation. The corresponding microstructure looks like an array of tubes or channels of holes aligned in the direction of the largest principal stress.

It would be tempting to assume that the 3-D result of Proposition 4.8 degenerates into the 2-D result of Proposition 4.7 in a plane stress situation, *i.e.*, when one of the principal stresses is equal to zero. That it is not so is the object of the following

Lemma 4.11 *In three dimensions, a plane stress τ with eigenvalues denoted by τ_1, τ_2, τ_3, such that*

$$\tau_1 = 0, \quad \tau_2 \neq 0, \quad \text{and } \tau_3 \neq 0,$$

is considered. Then,

$$g^*(\tau) = \frac{1}{2\mu}\left(\tau_2^2 + \tau_3^2\right) - \frac{\lambda}{2\mu(2\mu + 3\lambda)}\left(\tau_2 + \tau_3\right)^2 = A^{-1}\tau \cdot \tau, \tag{70}$$

and optimality is achieved by a rank-1 sequential laminate in the direction e_1, i.e.

$$m_1 = 1, \quad m_2 = 0, \quad m_3 = 0.$$

In this case the function $F(\tau, \theta)$ is simply

$$F(\tau, \theta) = \frac{1}{\theta} A^{-1}\tau \cdot \tau,$$

and the integrand F_ℓ coincides with the convex envelope of the original integrand f_ℓ when evaluated at τ.

The proof of Lemma 4.11 is immediate through inspection of the formulae in Proposition 4.8. From a practical standpoint, it has the consequence that, if we can use 3-D microstructures for solving a 2-D problem, then it is preferable to use a "varying thickness plate" approach (corresponding to the optimal rank-1 laminate) than a "plane Michell trusses" approach (corresponding the rank-2 laminates, optimal only in 2-D). Mathematically speaking, it means that, in a 2-D problem of shape optimization, the convexified formulation (obtained by laminating in the single direction orthogonal to the plane) lies below the quasi-convexified formulation (obtained by using only "in plane" rank-2 laminates); hence the qualitative differences that will be evidenced between 2-D and 3-D pictures: in 2-D the optimal microstructures look like a network of trusses or bars, while in 3-D they will appeal to either trusses or plates.

An other interesting limit case of Proposition 4.8 is that of a uni-axial stress. This is the purpose of the next lemma.

Lemma 4.12 *In three dimensions, a uni-axial stress τ with eigenvalues denoted by τ_1, τ_2, τ_3, such that*

$$\tau_1 = 0, \quad \tau_2 = 0, \quad \text{and } \tau_3 \neq 0,$$

is considered. Then,

$$g^*(\tau) = \frac{\mu+\lambda}{\mu(2\mu+3\lambda)}\tau_3^2 = A^{-1}\tau\cdot\tau, \tag{71}$$

and optimality is achieved by any rank-2 sequential laminate in the directions e_1, e_2, i.e., *any triplet* m_1, m_2, m_3 *with*

$$m_3 = 0,\ \ m_1 \geq 0,\ \ m_2 \geq 0,\ \ m_1 + m_2 = 1.$$

In this case again, $F(\tau,\theta) = \frac{1}{\theta}A^{-1}\tau\cdot\tau$, *and the integrand* F_ℓ *coincides with the convex envelope of the original integrand* f_ℓ *when evaluated at* τ.

The proof of Lemma 4.12 is also immediate by inspection of the formulae in Proposition 4.8. In a uni-axial stress setting, the optimal microstructure looks like an array of fibers aligned with the stress and any type of cross-sectional arrangement is admissible.

Another special case of Propositions 4.7 and 4.8 is that of hydrostatic stresses. A hydrostatic stress is of the form

$$\tau = pI_2,$$

where p is the pressure field. In such a case, concentric spheres assemblages provide another class of optimal microstructures for the lower bound in Theorem 4.2 or Corollary 4.4 (see [22]). The main interest of these assemblages is that no homogenization process is required when computing their effective properties. They are an example of "classical" optimal shapes in the original formulation whenever the boundary condition is a constant hydrostatic load. Furthermore, they are also an example of non-uniqueness of the optimal design.

A brief description of these concentric spheres constructions is given below, while we refer the reader to the classical treatise [14] for further details. Any smooth domain Ω can be covered by a so-called Vitali covering of spheres, *i.e.*, it can be completely filled by an infinite number of non-overlapping balls of all sizes. Of course, there is also an infinite number of such coverings. Then, in each sphere, a concentric spherical hole is cut, and its radius is determined in a manner such that the volume fraction of material is precisely θ. This yields a perforated domain Ω with infinitely many disjoint spherical holes of all sizes. It is a classical result that, for such a perforated domain under an hydrostatic boundary condition $f = pI_2$, the average stress is exactly equal to pI_2 and the average compliance is $\frac{Np^2}{\kappa^*}$ where κ^* is the so-called Hashin-Shtrikman upper bound on the bulk modulus [23]. In our context the following proposition is easily derived from Propositions 4.7 and 4.8.

Proposition 4.13 *For a hydrostatic stress* $\tau = pI_2$ *the optimal bound* $F(\tau,\theta)$, *defined by Corollary 4.4, reduces to*

$$F(pI_2,\theta) = \frac{Np^2}{\kappa^*},\ \ N = 2,3,$$

where κ^* *is the Hashin-Shtrikman upper bound on the bulk modulus defined by*

$$\frac{1}{N\kappa^* + 2(N-1)\mu} = \frac{\theta}{2(N-1)\mu} + \frac{1-\theta}{N\kappa + 2(N-1)\mu}.$$

Proposition 4.13 shows that $F(pI_2,\theta)$ coincides with the average compliance of the concentric spheres assemblage. In particular, it proves, first, that the concentric spheres construction is also optimal for the lower bound in Theorem 4.2, and second, that it is a solution of the optimal shape design (6) for the volume fraction θ. Remark that this type of "classical" optimal shapes would be very difficult to compute numerically. Indeed its boundary is very complex since it involves an infinite number of connected components on various length scales. Therefore, even in this case, the relaxed formulation is more practical from a numerical standpoint.

Our focus so far has been the case of a single energy or loading configuration. We investigate below the case of several energies. As before, we start from the classical result on the relaxation of $I_p(\ell,\eta)$ (see [5], [6], and Remark 2.4 for notation) which states that

$$F^{p,\eta}\left(\{\tau_i\},\theta\right) = \min_{A^*\in G_\theta^\eta} \sum_{i=1}^{p} {A^*}^{-1}\tau_i\cdot\tau_i, \tag{72}$$

where G_θ^η is again the set of all possible anisotropic Hooke's laws of composite materials obtained by mixing A and η in proportions θ and $1-\theta$. Formula (72) is refered to as an optimal lower bound on sum of p effective complementary energies. Once again (see [7]), the full G-closure set G_θ^η can be replaced by that of sequential laminates.

Theorem 4.14 *The optimal bound (72) is*

$$F^{p,\eta}\left(\{\tau_i\},\theta\right) = \min_{A^*\in L_\theta^\eta} \sum_{i=1}^{p} {A^*}^{-1}\tau_i\cdot\tau_i, \tag{73}$$

where L_θ^η is the set of all effective Hooke's laws of finite rank sequential laminates defined through (46). Furthermore, optimality in the right hand side of (73) is achieved, at most, by a rank-3 sequential laminate in 2-D, and by a rank-6 sequential laminate in 3-D.

Remark 4.15 *While the first part of Theorem 4.14 is nearly identical to the single load case explicited in Theorem 4.2, the second part is completely different (in 2-D the result is derived in [8], and in 3-D in [19]). The number of laminations does not depend on the number of energies p, but it is higher than for a single load. Furthermore, the lamination directions are not necessary aligned with the principal stress directions. This is a serious obstacle, and no explicit formulae are available as of yet for the computation of the optimal laminate in (73). In other words, the optimal microstructure has to be determined numerically rather than through an explicit formula.*

To deduce an expression for F^p from Theorem 4.14, we can now let η tend to zero in the lamination formula (46) to obtain the limit set L_θ^0 of sequential laminates defined by formula (48). We thus obtain

Corollary 4.16 *The function F^p, defined as the monotone limit of $F^{p,\eta}$ when η tends to zero, is given by*

$$F^{p}\left(\{\tau_i\},\theta\right) = \min_{A^*\in L_\theta^0} \sum_{i=1}^{p} {A^*}^{-1}\tau_i\cdot\tau_i. \tag{74}$$

Furthermore, since optimality is achieved for a finite rank sequential laminate, (74) becomes

$$F^p\left(\{\tau_i\},\theta\right) = \sum_{i=1}^{p} {A^*}^{-1}\tau_i\cdot\tau_i + \frac{1-\theta}{\theta} g_p^*\left(\{\tau_i\}\right), \tag{75}$$

where g_p^* is a continuous and convex function of $\{\tau_i\}$, homogeneous of degree 2, strictly positive when at least one $\tau_i \neq 0$.

The above result is very similar to Corollary 4.4 and their proofs are parallel. The major difference is that we do not have an explicit formula for g_p^*. Indeed in view of the lamination formula (48) and Theorem 4.14, g_p^* is obtained as the result of an optimization *not only* on the parameters m_i, *but also* on the lamination directions. We have been unable to perform this optimization by hand, and in future numerical computations we will rely on a numerical procedure for the optimization of the laminate microstructure.

5 A numerical algorithm for 2 and 3-dimensional shape optimization.

5.1 description of the algorithm

This section presents the proposed numerical algorithm for shape optimization, which is based on the homogenization method as already announced in [4]. The key idea is to compute "generalized" optimal shapes for the relaxed formulation, rather than "classical" shapes which are merely approximately optimal for the original formulation. We thus begin by recalling the relaxed formulation as computed in Sections 3 and 4 above. The objective function is

$$I^*(\ell) := \min_{\tau\in\Sigma(\Omega)} \int_\Omega F_\ell(\tau)dx, \tag{76}$$

where

$$F_\ell(\tau) = \min_{0\leq\theta\leq 1}\left\{\min_{A^*\in L_\theta^0} {A^*}^{-1}\tau\cdot\tau + \ell\theta\right\}, \tag{77}$$

and $\Sigma(\Omega)$ is the set of statically admissible stresses defined by

$$\Sigma(\Omega) = \left\{\tau \in L^2(\Omega; I\!R_s^{N^2}) \mid \ div\ \tau = 0 \text{ in } \Omega;\ \ \tau\cdot n = f \text{ on } \partial\Omega\right\}. \tag{78}$$

Furthermore, in Section 4 we performed an explicit computation of the minimizer A^* in the right hand side of (77), in two or three dimensions.

The relaxed formulation (76)–(78) evokes a problem of nonlinear elasticity. The optimal density (a "generalized" shape) is recovered by the optimality condition on θ in equation (77). A simple algorithm solves, in a first step, this nonlinear minimization problem in the stress τ, by using, e.g., a conjugate gradient method. In a second step an optimal density θ is recovered through the optimality condition. Such an approach has been implemented in [6] for the 2-D case, but it is not completely satisfactory for the following reasons. As in all computations involving complementary energies, high degree finite elements have to be used for stress accuracy. The resulting computations are very costly and limited, in practice, to a two dimensional setting. Furthermore, the highly non-trivial energy F_ℓ is not smooth at $\tau = 0$ which calls for special care in the gradient method. Convergence to the minimum is usually fairly slow.

Therefore, we prefer another algorithm, the so-called "alternate directions method", that we now describe. It is based on two key ideas. The first one is to consider the relaxed problem $I^*(\ell)$ as a minimization problem not only for the stress, but also for the structural parameters, the density θ, and the microstructure A^*. The second key idea is not to try to minimize directly in the triplet of variables (τ, θ, A^*), but rather to adopt an iterative approach and minimize separately and successively in the design variables (θ, A^*) and in the field variable τ. The minimization in τ for fixed design variables amounts to the resolution of a problem of linear elasticity for the structure defined by the previous design variables. The minimization in (θ, A^*) for a fixed stress field is explicit in view of the formulae obtained in the previous section. Consequently, the algorithm is structured as follows:

1. Initialization of the design parameters (θ_0, A_0^*) (for example, taking $\theta_0 = 1$ and $A_0^* = A$ everywhere in the domain).
2. Iteration until convergence:
   (a) Computation of τ_n through a problem of linear elasticity with $(\theta_{n-1}, A_{n-1}^*)$ as design variables.
   (b) Updating of the design variables (θ_n, A_n^*) by using the stress τ_n in the explicit optimality formulae of Section 4.

Convergence of this iterative algorithm is detected when the objective function becomes stationary, or when the change in the design variables becomes smaller than some preset threshold. Notice that the above iterative process always decreases the value of the objective function at each iteration. Indeed, since A_n^* minimizes the compliance under the stress field τ_n, and since τ_{n+1} minimizes the elastic complementary energy corresponding to the Hooke's law A_n^*, it follows that

$$
\begin{aligned}
\int_\Omega (A_{n-1}^*)^{-1}\tau_n \cdot \tau_n dx + \ell \int_\Omega \theta_{n-1} dx &\geq \int_\Omega (A_n^*)^{-1}\tau_n \cdot \tau_n dx + \ell \int_\Omega \theta_n dx \\
&\geq \int_\Omega (A_n^*)^{-1}\tau_{n+1} \cdot \tau_{n+1} dx + \ell \int_\Omega \theta_n dx \ .
\end{aligned}
$$

Remark 5.1 *The alternate direction algorithm is apparented to the two previously known methods: that of [11], [36], and that of [6]. As already mentioned, the latter considers the relaxed problem $I^*(\ell)$ as a problem of nonlinear elasticity. The former transforms the minimization over statically admissible stresses into a maximization over displacements, and (76) becomes*

$$
I^*(\ell) := \min_{0\leq\theta\leq 1} \min_{A^*\in L^0_\theta} \max_{u\in H^1(\Omega)^N} \left\{ 2\int_{\partial\Omega} f\cdot u ds - \int_\Omega A^* e(u)\cdot e(u) dx + \ell \int_\Omega \theta dx \right\}, \qquad (79)
$$

where $e(u)$ is the strain tensor $(\nabla u + \nabla^t u)/2$. The ensuing numerical scheme is based on the first order optimality conditions at the saddle point of the functional (79). This leads to a rather intricate updating process for the design variables (volume fraction of material θ and the individual volume fractions and orientations of each layer). The computation is also performed using alternate directions; firstly the solution u of a problem of linear elasticity where all design variables are fixed is obtained, then the design variables are updated using the optimality criterion. The existence of a saddle point for the $\min_{A^* \in L^0_\theta} max_{u \in H^1(\Omega)^N}$ problem 79 is established in Theorem 4.1 of [27]; note however that, in the resulting formulation, the minimization in θ must be performed last.

the min-max problem (79) is not guaranteed since the integrand does not satisfy any concave-convex type condition.

5.2 A few technical algorithmic issues

Convergence criterion:
The successive problems of linear elasticity are solved by the finite element method. We use quadrangular *Q1* elements for the displacements while the stresses τ_n and their principal directions and principal values, are computed at the center of each element. The parameters for the optimal laminate are then computed in each cell using formulae (54) in two dimensions, or (60-65) in three dimensions. The Hooke's law for the optimal laminate is computed with the help of Lemma 4.5.

The procedure is iterated until the quantity

$$\max \left(\max_i (|\theta_i^{n+1} - \theta_i^n|), 1 - \frac{\int_\Omega (A^*_{n+1})^{-1} \tau^{n+1}.\tau^{n+1} + \ell \int_\Omega \theta^{n+1}}{\int_\Omega (A^*_n)^{-1} \tau^n.\tau^n + \ell \int_\Omega \theta^n} \right)$$

becomes smaller than a preset threshold. About 100 iterations are required to reach a criterion of 10^{-5}. On Figure 3, the evolution of the objective function in a typical calculation is plotted. Other convergence criteria could be used, for instance the L^2 norm of $\tau^{n+1} - \tau^n$.

Volume constraint:
In most of the computations presented here, the Lagrange multiplier ℓ is held at a fixed value. Ideally, one could perform several calculations with different values of ℓ, then try to adjust this parameter in order to match a given constraint on the volume. As we explained in Section 3, we do not know how to determine ℓ beforehand. As an alternative, computations were also performed, where ℓ is adjusted at each iteration, so that the corresponding value of the optimal density satisfies the volume constraint. In other words, once the stress τ_n is computed, we determine θ_n and ℓ_n by solving

$$\theta_n = \min\{1, \sqrt{\frac{g^*(\tau_n)}{\ell_n}}\} \qquad \int_\Omega \theta_n = \Theta$$

through a simple iterative procedure.

Singularities in the composite Hooke's law:
The generalized Hooke's laws computed at each iteration turn out to be singular, an undesired feature when solving problems of linear elasticity. This singular behavior has several sources.

First, we note that the effective tensor is equal to zero when the density vanishes. Implicitely, the corresponding stress field should vanish simultaneously. This problem, which occurs in 2 and 3-D, is easily circumvented by imposing a positive threshold on the density. In practice, the smallest admissible value of θ is fixed at 10^{-3}. Numerical experiments suggest that the choice of 10^{-3} is not important.

We also remark that rank-1 and rank-2 laminates produce degenerate Hooke's laws (*cf.* Remark 4.6). In 3-D, the proportions m_i are forced to be greater than zero. Consequently, the algorithm only uses rank-3 laminates, which are non-singular.

In 2-D, rank-1 laminates are eliminated like in the 3-D case. However, the algorithm uses rank-2 laminates as optimal microstructures. The singularity is avoided by adding a small correction term to the composite Hooke's law.

We describe three attempted regularizations of rank-2 laminates, in the case where the principal directions of τ coincide with $OxOy$ (the other cases follow by rotation). The elasticity tensor of the corresponding rank-2 laminate only has the following non-zero coefficients

$$\begin{aligned}
A^*_{1111} &= \frac{4\kappa\mu(\kappa+\mu)\theta(1-\theta m_2)m_2}{4\kappa\mu\ m_1 m_2\theta^2 - (\kappa+\mu)^2(1-\theta)} \\
A^*_{1122} = A^*_{2211} &= \frac{4\kappa\mu(\kappa-\mu)\theta^2 m_1 m_2}{4\kappa\mu\ m_1 m_2\theta^2 - (\kappa+\mu)^2(1-\theta)} \\
A^*_{2222} &= \frac{4\kappa\mu(\kappa+\mu)\theta(1-\theta m_1)m_1}{4\kappa\mu\ m_1 m_2\theta^2 - (\kappa+\mu)^2(1-\theta)} \ .
\end{aligned}$$

The first method of correction simply amounts to replacing $A^*_{1212} = A^*_{1221} = A^*_{2112} = A^*_{2121}$ by $2\mu\delta$, where δ is "small". The second method consists in replacing A^*, by the optimal laminate corresponding to a mixture of A and δA, *i.e.*, by a configuration that achieves the minimum of $F^{\delta A}(\tau,\theta)$, in the particular case where the soft material is proportional to A. This simplifies the computations of the optimal Hooke's law which is non-singular. The third regularization, corresponds to the 2-D projection of a rank-3 laminate, with laminations along Ox, Oy, Oz in proportions $(1-\delta)m_1, (1-\delta)m_2$ and δ respectively. The resulting elasticity tensors are easily computed with the formulae from Section 4.

Numerical experiments suggest that the three corrections give comparable results although the second one is slightly better and converges faster. Computational runs suggest that when the coefficient δ is too small, the algorithm may select a wrong solution, possibly a local minimum. In practice we use $\delta = 10^{-2}$.

Checkerboard instabilities:
Our algorithm is subject to checkerboard instabilities for the density θ similar to those reported in [10],[24],[25]. These instabilities do not appear if the displacements are computed using higher order elements (*Q2* in our case), while the lamination parameters are

computed with only piecewise constant stresses. Note, however, that *Q2* elements are expensive for very fine meshes and for 3-D calculations.

The numerical onset of checkerboard patterns is still mysterious, although it is worth noticing that piecewise constant stresses, which are equilibrated with respect to deformation fields of *Q1*-displacements, are checkerboard-like. In practice, such instabilities only appear after a large number of iterations, when the convergence criterion is very tight (cf. Figure 5).

In 2-D calculations, we eliminate these instabilities with a method used to filter the pressure in a Stokes flow computation [12]. Once the piecewise constant optimal densities θ_i^n are determined, we project them on super-elements, which are clusters of 4 adjacent elements, so as to eliminate the checkerboard mode and preserve the overall density. We have not experienced any checkerboard patterns in 3-D calculations, and all the examples shown below have been computed without filtering.

6 Penalization of intermediate densities.

As explained in Section 5, our numerical algorithm for computing optimal design is based on the relaxed formulation introduced in Section 2. The numerical computations deliver relaxed, or generalized, optimal shapes – a density of material – rather than classical optimal shapes for the original formulation – a characteristic function of the material domain. In other words, our method produces a layout of material, which, as expected, includes large regions of composite materials with intermediate density. From a practical standpoint, this is an undesirable feature since the primary goal is to find a real shape – a density taking only the values 0 or 1! This drawback is avoided through a post-processing technique that *penalizes* composite regions. The goal is to deduce, from the optimal densities, a quasi-optimal shape. In loose terms, the solution of the relaxed problem is projected onto the set of classical solutions of the original problem, in the hope that the value of the objective functional will not increase too much in the process.

The strategy is as follows. Upon convergence to an optimal density, we run a few more iterations of our algorithm where we *force* the density to take values close to 0 or 1. This changes the optimal density and produces a quasi-optimal shape. Of course, the procedure is purely numerical and mesh dependent. The finer the mesh, the more detailed the resulting structure will appear at the outset of the penalization process. The method works well, because the relaxed design is characterized not only by a density θ but also by a microstructure A^*, which is hidden at the sub-mesh level. The penalization tends to reproduce the microstructure at the mesh level.

Two penalization techniques for the intermediate composite densities have been used. Both amount to a modification of the explicit formula (24) that expresses the optimal density in terms of the stress. Specifically, instead of updating the density with the true optimal density θ_{opt}, a value θ_{pen} is used. Our first choice for θ_{pen}, already described in [2], [4], is

$$\theta_{pen} = \frac{1-\cos(\pi\theta_{opt})}{2}.$$

The choice of a cosine function for the penalized density is arbitrary. If θ_{pen} is too close to θ_{opt}, the scheme is insensitive to the proposed penalization, while if θ_{pen} is forced too close to 0 or 1, the fine patterns of the shape are destroyed.

In the context of plate thickness optimization, another technique has been proposed [9],[40]. It consists in setting

$$\theta_{pen} = (\theta_{opt}^2/p)^{1/(1+p)} \text{ for some } p < 1.$$

This alternate choice also gives good results. It corresponds to the optimal value of θ for a modified integrand, namely

$$F_{p,\ell}(\tau) \quad := \quad \min_{0\leq\theta\leq 1} \{F(\tau,\theta) + \ell\theta^p\} \quad ,$$

which is supposed to take into account "manufacturing costs" of perforated materials (the "cost" of intermediate densities increases in (80) as p decreases from 1 to 0).

7 Quasiconvexification versus convexification.

This section is devoted to a comparison of the relaxed formulation introduced in Section 2 with the convexification of the original problem. Such a comparative study is motivated by the occasional use of the convexified formulation for the computation of optimal shapes, under the name of "fictitious material approach" (see e.g. [30], [35]). Let us briefly describe the argument. When combined with the penalization procedure, the numerical algorithms for computing optimal shapes – based on the relaxed formulation – may seem self-defeating. Homogenization theory is introduced, proper optimal microstructures, and complicated formulae for updating the design variables are laboriously derived, and yet, in the end, this wealth of information is seemingly wasted through the penalization process! A natural idea is thus to propose a simpler approach based on the *convexification* of the original problem (which is easily computed, see below), coupled with the same penalization procedure, as described in Section 6. The advantages of the approach are the following: the layout optimization problem still becomes a sizing optimization problem, *i.e.*, shapes are replaced by densities. Implementation is straightforward since the convexified formulation is very simple, no knowledge of homogenization or composite materials is required and, in 2-D, the method relies on the physical notion of "varying thickness" plates. Although comparable results are produced in a few test cases, the method is much more sensitive to the penalization and it usually yields worse results than those of the homogenization (or relaxed) method.

The "fictitious material" approach considers the following state equation

$$\begin{cases} \sigma = \theta(x)Ae(u) & e(u) = \left(\nabla u + \nabla^t u\right)/2 \\ div\ \sigma = 0 & \text{in } \Omega \\ \sigma \cdot n = f & \text{on } \partial\Omega, \end{cases}$$

where $\theta(x)$ is a density function with values between 0 and 1. The goal is to minimize, over all the possible densities, the weighted sum of the compliance and of the weight. Thus we set

$$CI(\ell) := \inf_{\theta(x)\in L^\infty(\Omega;[0,1])} \left(c(\theta) + \ell \int_\Omega \theta(x) \right),$$

where the compliance is defined by

$$c(\theta) = \int_{\partial\Omega} f \cdot u = \int_{\Omega} < (\theta(x)A)^{-1}\sigma, \sigma > .$$

Upon using the principle of complementary energy and switching the two minimizations, the following equivalent formulation is derived:

$$CI(\ell) = \inf_{\sigma \in \Sigma(\Omega)} \int_{\Omega} Cf_{\ell}(\tau) dx, \tag{80}$$

where Cf_{ℓ} is the convex envelope of the function f_{ℓ}, *cf.* (14),

$$Cf_{\ell}(\tau) = \begin{cases} A^{-1}\tau \cdot \tau + \ell & \text{if } A^{-1}\tau \cdot \tau \geq \ell, \\ 2\sqrt{\ell A^{-1}\tau \cdot \tau} & \text{if } A^{-1}\tau \cdot \tau \leq \ell, \end{cases}$$

and $\Sigma(\Omega)$ is defined in (13).

Formulation (80) is called the convexification of the original problem (8) or (12). Since it is a convex minimization problem, the existence of minimizers is straightforward and the infimum in (80) is a minimum. Recall that the original formulation is

$$I(\ell) = \inf_{\sigma \in \Sigma(\Omega)} \int_{\Omega} f_{\ell}(\tau) dx,$$

while the relaxed (or homogenized) formulation is

$$I^*(\ell) = \inf_{\sigma \in \Sigma(\Omega)} \int_{\Omega} Qf_{\ell}(\tau) dx,$$

where Qf_{ℓ} is the quasi-convex envelope of f_{ℓ} (see (33)). Furthermore,

$$f_{\ell}(\tau) \geq Qf_{\ell}(\tau) \geq Cf_{\ell}(\tau),$$

where the inequalities are strict for most choices of the stress τ. Notice, however, that

$$I(\ell) = I^*(\ell) \geq CI(\ell) \ .$$

We have numerically implemented the convex formulation with the “alternate directions” strategy described in Section 5. For a given density θ, we compute the stress τ solution to the linear elasticity state equation, then update the design variable θ using the optimality relation

$$\theta(x) = \begin{cases} 1 & \text{if } A^{-1}\tau \cdot \tau \geq \ell, \\ \sqrt{\ell^{-1} A^{-1}\tau \cdot \tau} & \text{if } A^{-1}\tau \cdot \tau \leq \ell. \end{cases}$$

The algorithm converges quickly and smoothly and we supplement it with the penalization procedure of Section 6. A few numerical results are displayed in Section 8.2 and compared with those of the homogenization method. The fictitious penalized designs are qualitatively comparable to their homogenized counterparts, but they lack the complexity and pattern details.

The absence of implicit sub-mesh microstructures explains the lower performance of the fictitious material approach. Loosely speaking, the convex formulation has a single free design parameter – the density θ – while the homogenized, or relaxed, formulation has more parameters – θ and the microstructure A^* – allowing for greater flexibility in the design of optimal shapes.

Remark 7.1 *As already pointed out, in a 2-D setting the convexified formulation (80) can be viewed as a variable thickness approach for a plate. This is formalized in Lemma 4.11, which claims that, in a plane stress problem, the three-dimensional relaxed formulation coincides with the two-dimensional convexified formulation. In other words, the optimal microstructure is everywhere a rank-1 layering in the x_1 direction – a varying thickness plate – if the boundary conditions are such that the solution of the 3-D relaxed formulation does not depend on the first space variable x_1. Also, in this case, the 3-D relaxed energy $Qf_\ell(0, \tau_2, \tau_3)$ is exactly equal to the 2-D convex energy $Cf_\ell(\tau_2, \tau_3)$. When departing from a plane stress setting, the convexified formulation (80) has no physical meaning.*

8 Numerical results.

In this section, we present several numerical examples which illustrate various aspects of the method. The workspace Ω is discretized with quadrangular elements in 2-D and hexaedral elements in 3-D. The displacement is approximated by $Q1$ interpolation and the resulting stress field is averaged on each cell.

All the computations are performed with the bulk modulus κ and the shear modulus 2μ equal to 1. The smallest admissible value of θ and of the proportions m_i is 10^{-3}, in order to avoid very low proportions. In practice, the value of this parameter is insignificant; any small number produces similar results. The density θ is represented with a gray scale: areas where $\theta = 1$ (pure material) are black, whereas white zones correspond to voids. The calculations are initialized with the most rigid shape, *i.e.*, $\theta_0 = 1$, $A_0^* = A$ everywhere in Ω. We attempted several computations with other initial shapes and obtained very similar designs. The method seems stable with respect to the choice of initial configuration, although the number of iterations required for convergence may be greatly affected. This stability might be an indication of uniqueness of the optimal composite solution, at least within the class of rank-2 laminates, for the tested problems (workspace, boundary conditions and loading). Further tests are in progress for problems where non-uniqueness of the optimal generalized shape is known.

8.1 The cantilever 1.6:

This example has already been investigated by several authors, and it has become a sort of benchmark for layout optimization algorithms. The workspace Ω is a rectangle of dimensions 1.6×1 discretized with a 4000 element mesh. The object to be found is submitted to a vertical point load applied at the middle of the right vertical side, while the left side is clamped. Similar designs would have been obtained under a uniform traction on a small part of the side instead of a point load.

Figure 1 shows the output of the algorithm after 30 iterations. Although one can guess a "shape" on the edges of the structure, its center contains a large composite zone. Figure 3 represents the objective function history for this calculation. The corresponding penalized shape is shown in Figure 2. Most of the gray material has been removed, while the difference in the objective function is only three to four percent. In particular, the fuzzy center has been replaced by a bar structure reminiscent of a Michell truss.

If the previous non-penalized computation is continued, checkerboard patterns are produced (cf. Figure 4). Their appearance can be detected on the plot of the objective function, Figure 5. Indeed, one remarks a sharp decrease after the first iteration, and stabilization around a specific value after $5-10$ iterations. After sufficiently many iterations, the objective function decreases again, with the onset of checkerboard instabilities. On Figure 5, the objective function is also plotted for a computation with filtering.

8.2 The bridge arch:

In this example, the workspace is a 2×1.2 rectangle. The structure is simply supported at the edges of its base, on a zone of width $1/16$. A vertical point load is applied at the middle of the lower side. Since the applied forces, the initial configuration and the boundary conditions are symmetric, a symmetric solution is expected and the computations are performed on half of the domain only. Figures 6.a-c show the resulting composite design, for different mesh sizes (1080, 4320 and 17280 elements). Figures 7.a-c display the corresponding penalized designs. The composite designs are stable with respect to refinement of the mesh, whereas, as expected, the number of fine structures appearing after penalization strongly depends on the discretization.

We also compared the relaxed formulation to the convexified one (cf. Section 7). Figure 8.a-b show the output of the alternate directions algorithm for the convexified functional and the corresponding penalized design (the mesh is that of Figure 6.b). The objective function histories of Figure 10 demonstrate that the performance of the latter design is worse than that of the penalized design obtained through relaxation. Similarly, Figure 9 shows the design resulting from a penalization of composites from the beginning of the computation. The resulting objective function is significantly higher, as evidenced in Figure 9.

8.3 The 3-D cantilever 1.6:

This is the 3-D analog of the first example. The workspace is a $1.6 \times 0.8 \times 1$ box, clamped at the right vertical side. A point load is applied in the middle of the opposite face. We used a mesh of 19200 elements and started from an initial configuration with $\theta_0 = 1$ throughout. The algorithm produces a symmetric layout, which permits to compute a half domain only.

The 3-D pictures are harder to visualize. Figure 11.a represents the iso-surface $\theta \geq 0.3$ of composite density. In this example, the iso-surfaces are smooth and embedded into each other as θ increases. The next picture (Figure 11.b) shows the design after penalization, the effect of which is to cluster the available material in plate-like or bar-like components: here, a thin vertical plate (with a width of only one element) increases the rigidity of the center-part, whereas 3-D trusses reproduce patterns similar to the 2-D design (cf. Figure 2).

8.4 The 3-D electric masts:

This example is an attempt to compute a more realistic structure. The workspace is a T-like box. Two symmetric vertical loads are applied in the middle of the lower edges of the horizontal part of the T and represent the force exerted by the wires on the mast. Simply supported boundary conditions are imposed at the corners of the base of the T. In the calculations, the computed shapes are forced to occupy 15% of the total volume.

Only a quarter of the object is computed, by virtue of the symmetries. The first calculation (Figure 12.a-b) represents the composite, resp. penalized designs, produced by our algorithm for a T-box with a $80 \times 40 \times 46$ bar and a $40 \times 40 \times 80$ foot, using a mesh with 14976 hexaedral elements. As in the case of the 2-D bridge, the algorithm builds a quasi-circular arch to connect both edges of the T. The horizontal bars that link the feet of the mast in the penalized design do not appear in the composite picture. Remark that the penalization produces a bar-like design that evokes the shape of existing electric masts. As explained above, the number of such bars depends of the mesh, but also on the size of the workspace. An "industrial" computation would require a finer mesh, and a larger workspace in the z-direction.

Figures 13.a-b, show the resulting designs for a T-box with a $80 \times 20 \times 20$ bar and a $40 \times 20 \times 80$ base, meshed with 24000 hexaedral elements. The algorithm could no longer build an arch as before, and it creates a plate-like dome. The computation took about three days on a HP9000/755.

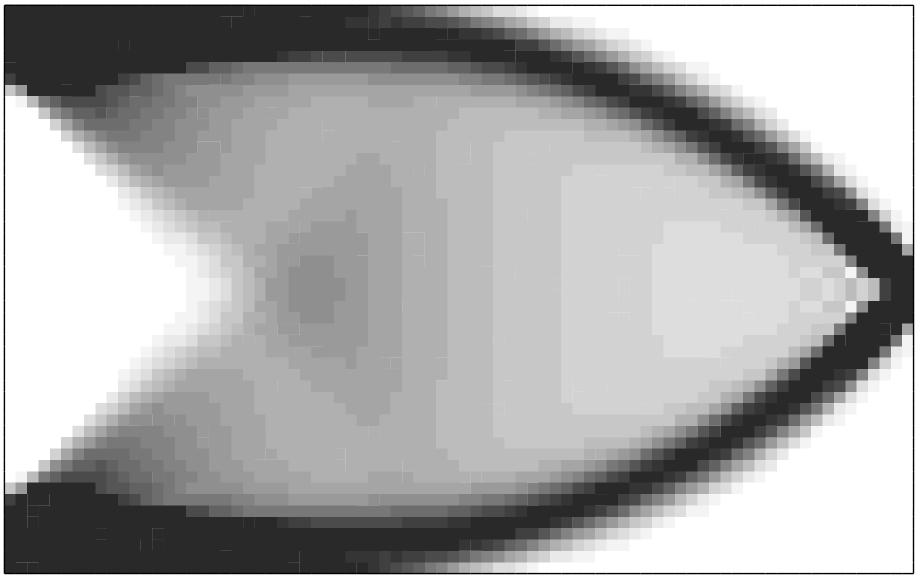

Figure 1: *cantilever: composite design.*

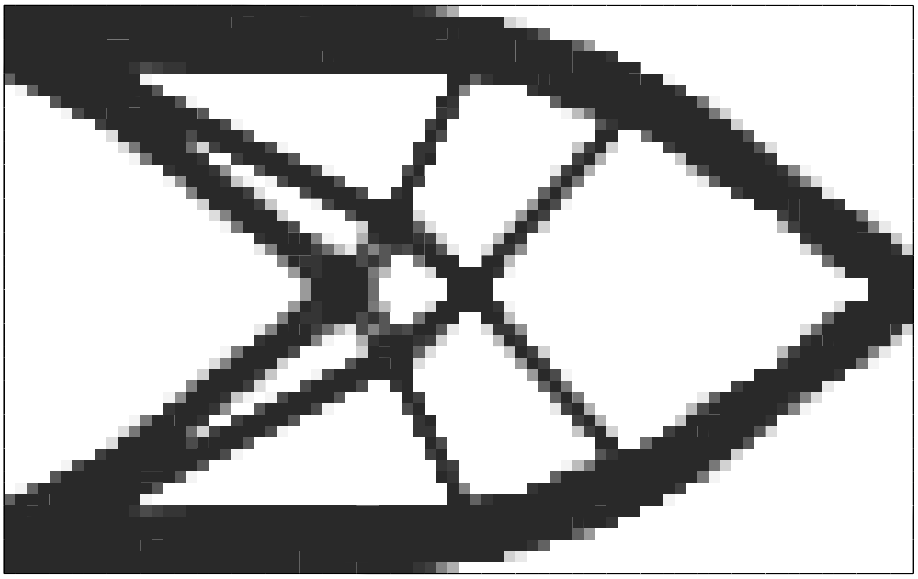

Figure 2: *cantilever: penalized design.*

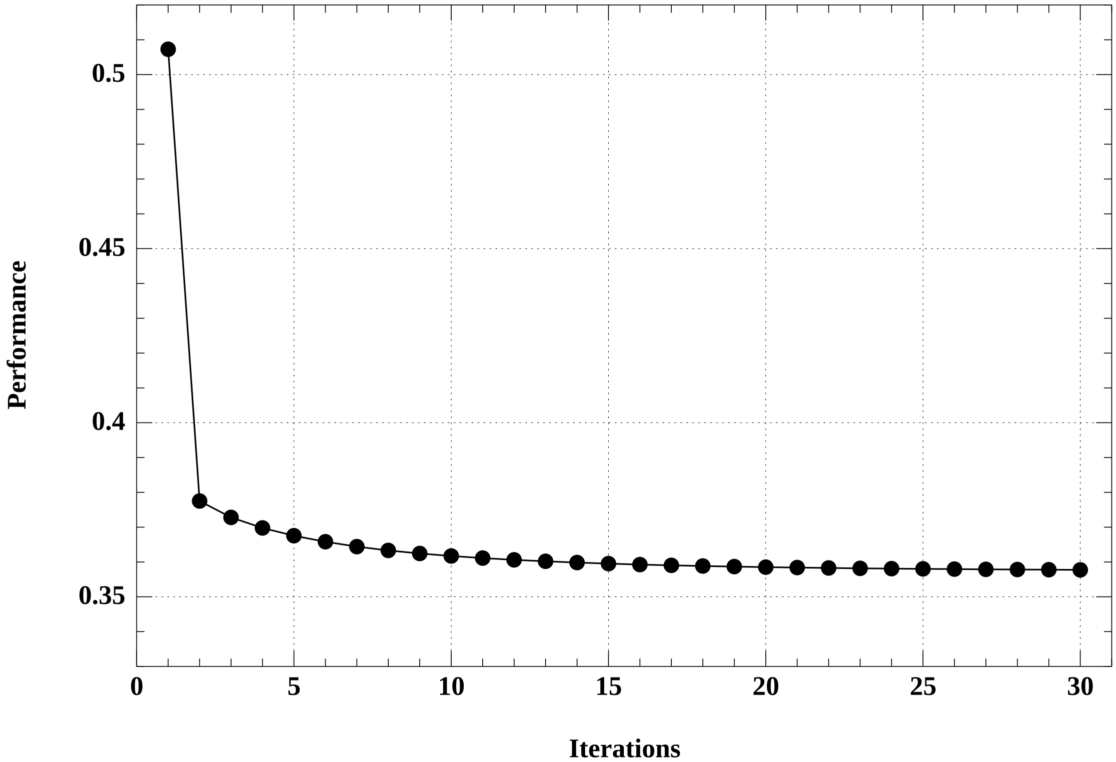

Figure 3: *typical convergence history.*

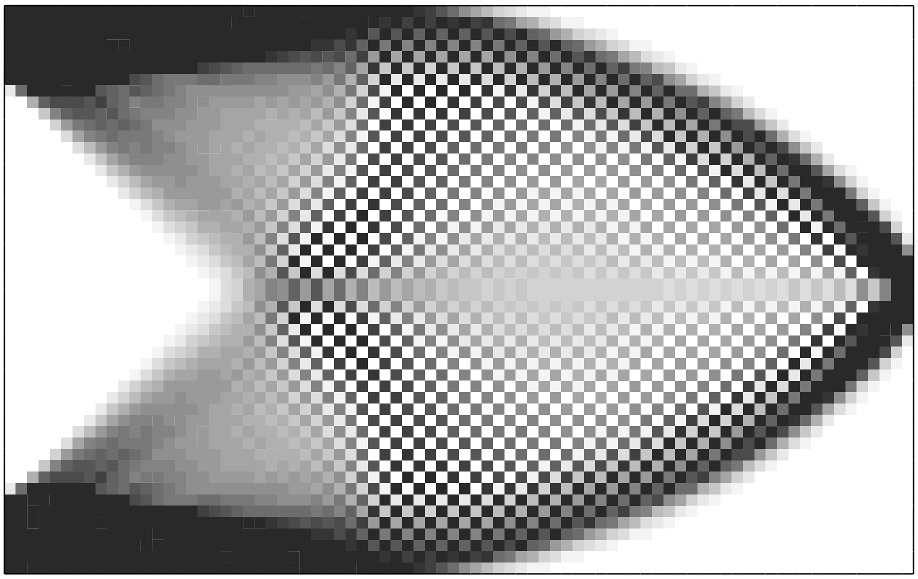

Figure 4: *cantilever: checkerboard patterns.*

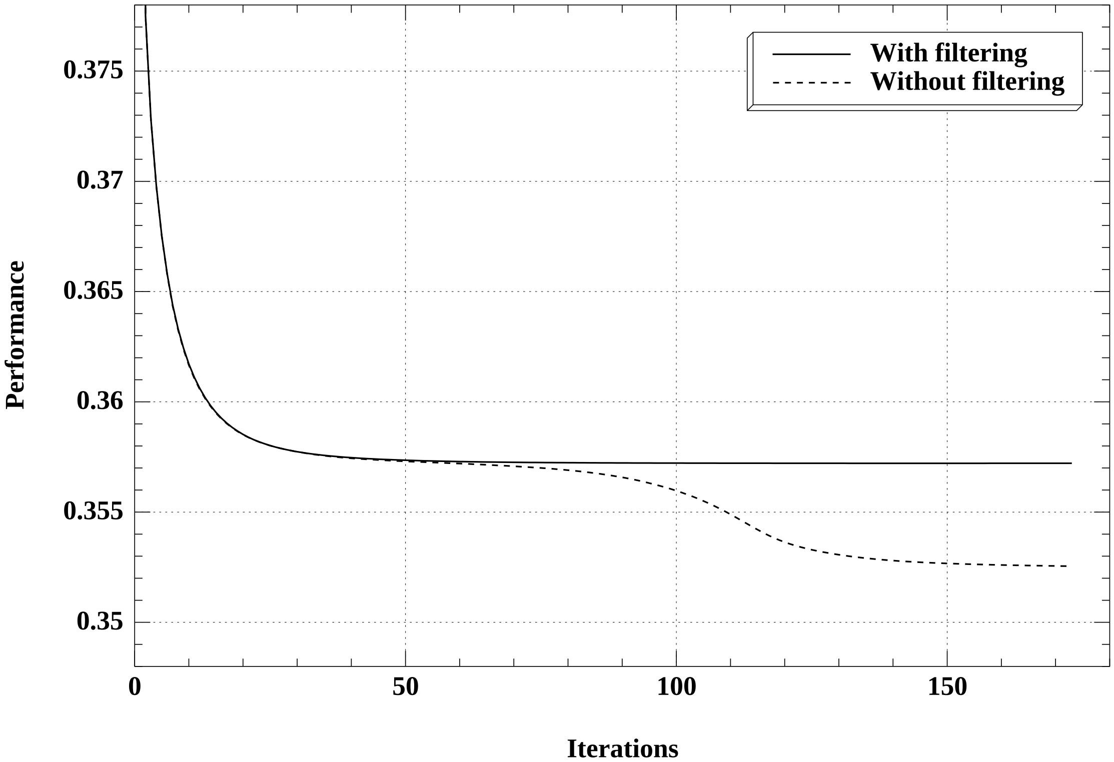

Figure 5: *convergence history showing the appearance of checkerboard patterns.*

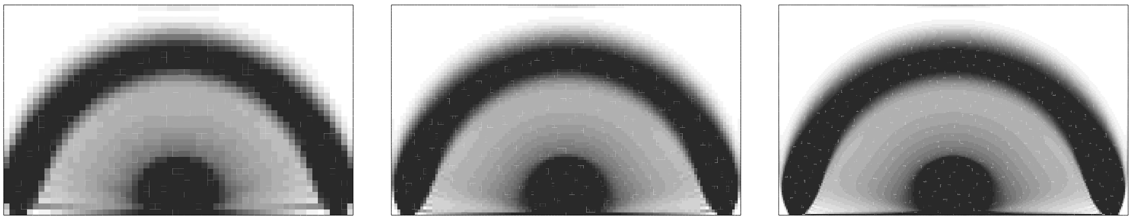

Figure 6: *bridge arch: composite design for different mesh sizes.*

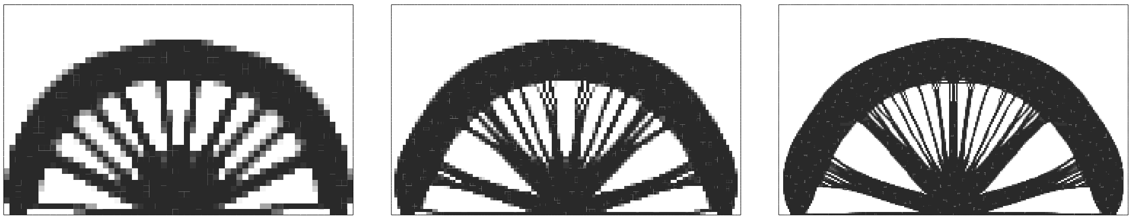

Figure 7: *bridge arch: design for different mesh sizes after penalization.*

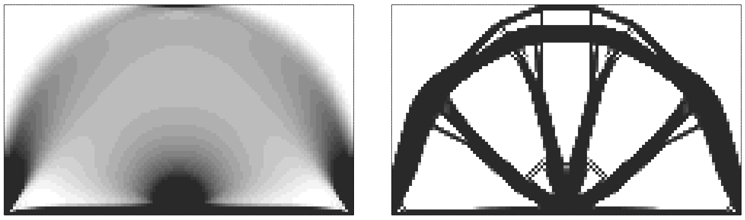

Figure 8: *bridge arch resulting from optimizing the convexified functional; fictitious composite solution (left) and penalized (right).*

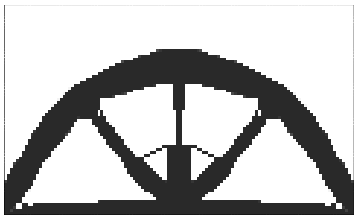

Figure 9: *bridge arch resulting from penalizing the composites from the start of the algorithm.*

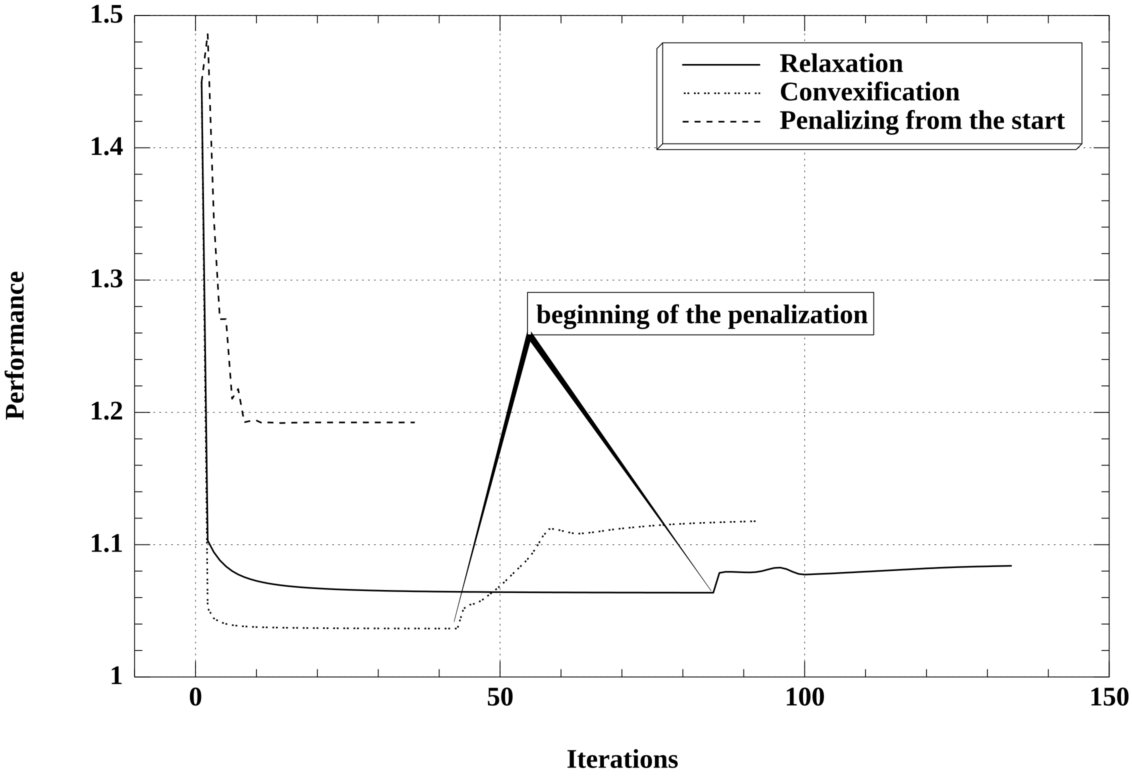

Figure 10: *Convergence history: relaxation vs. convexification.*

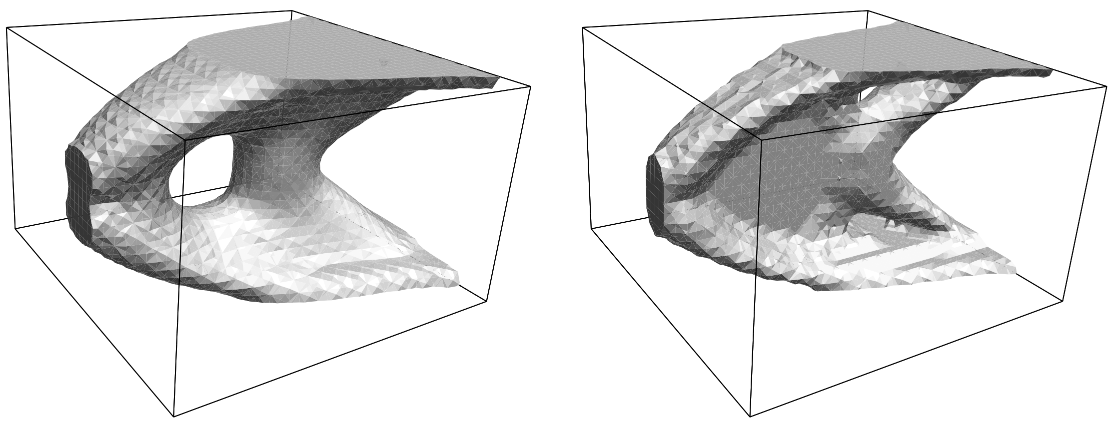

Figure 11: *3-D cantilever: composite solution (left) and penalized (right).*

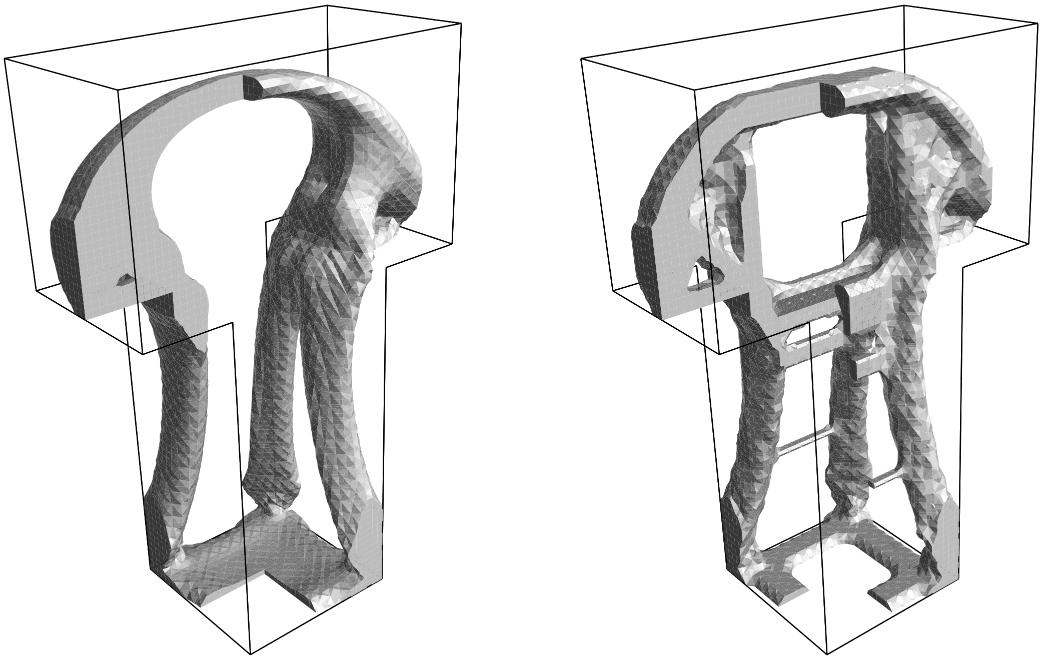

Figure 12: *electric masts: composite solution (left) and penalized (right).*

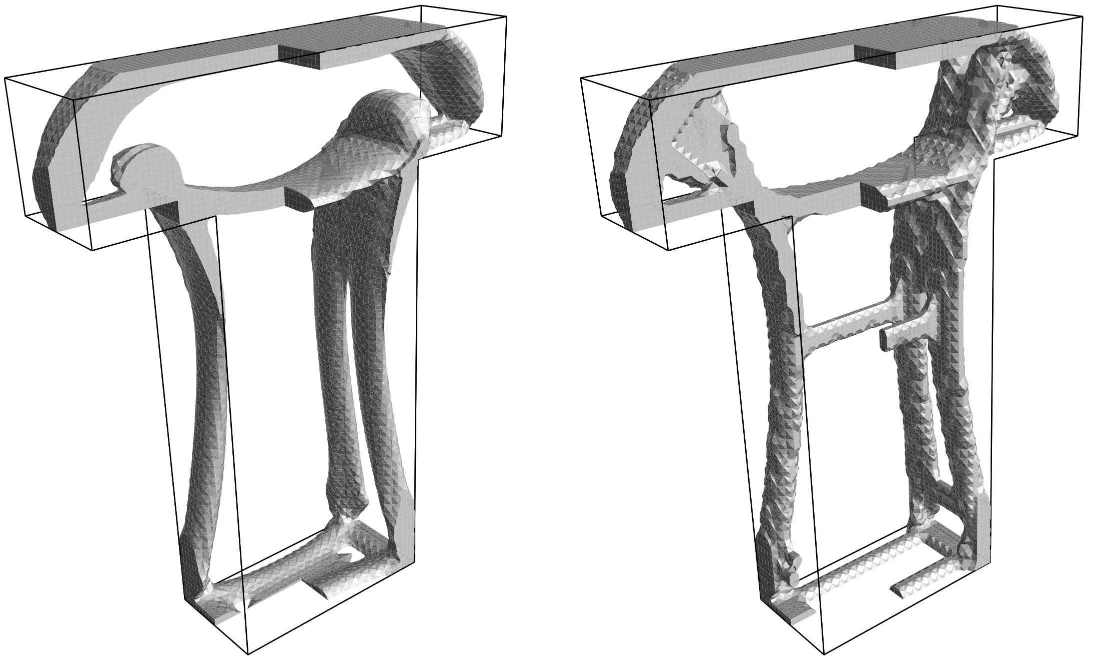

Figure 13: *electric masts: composite solution (left) and penalized (right).*

References

[1] F. Acerbi, N. Fusco, *Semicontinuity Problems in the Calculus of Variations,* Arch. Rat. Mech. Anal. 86, 125–145 (1984).

[2] G. Allaire, *Structural optimization using optimal microstructures,* In "MECAMAT 93 International Seminar on Micromechanics of Materials", Collection de la Direction des Etudes et Recherches d'Electricité de France, Eyrolles, Paris (1993).

[3] G. Allaire, *Explicit lamination parameters for three-dimensional shape optimization,* Control and Cybernetics 23, 309–326 (1994).

[4] G. Allaire, G. Francfort, *A numerical algorithm for topology and shape optimization,* In *Topology design of structures*, Nato ASI Series E, M. Bendsoe et al. eds., 239–248, Kluwer, Dordrecht (1993).

[5] G. Allaire, R.V. Kohn, *Optimal bounds on the effective behavior of a mixture of two well-ordered elastic materials,* Quat. Appl. Math. 51, 643–674 (1993).

[6] G. Allaire, R.V. Kohn, *Optimal design for minimum weight and compliance in plane stress using extremal microstructures,* Europ. J. Mech. A/Solids 12, 6, 839–878 (1993).

[7] M. Avellaneda, *Optimal bounds and microgeometries for elastic two-phase composites,* SIAM J. Appl. Math., 47, 6, 1216–1228 (1987).

[8] M. Avellaneda, G. Milton, *Bounds on the effective elasticity tensor of composites based on two point correlations,* in Proceedings of the ASME Energy Technology Conference and Exposition, Houston, 1989, D. Hui et al. eds., ASME Press, New York (1989).

[9] M. Bendsoe, *Optimal shape design as a material distribution problem,* Struct. Optim., 1, 193–202 (1989).

[10] M. Bendsoe, A. Diaz, N. Kikuchi, *Topology and generalized layout optimization of structures,* In *Topology Optimization of Structures*, Nato ASI Series E, M. Bendsoe et al. eds., 159–205, Kluwer, Dordrecht (1993)

[11] M. Bendsoe, N. Kikuchi, *Generating Optimal Topologies in Structural Design Using a Homogenization Method,* Comp. Meth. Appl. Mech. Eng., 71, 197–224 (1988).

[12] F. Brezzi, M. Fortin, *Mixed and hybrid Finite Element Methods,* Springer, Berlin, 1991.

[13] A. Cherkaev, R. Palais, *Optimal design of three-dimensional axisymmetric elastic structures,* to appear.

[14] R. Christensen, *Mechanics of composite materials,* John Wiley, New York (1979).

[15] B. Dacorogna, *Direct Methods in the Calculus of Variations,* Springer, New York (1989).

[16] G. Dal Maso, R. Kohn, *The local character of G-closure,* in preparation.

[17] I. Fonseca, S. Müller, to appear.

[18] G. Francfort, F. Murat, *Homogenization and Optimal Bounds in Linear Elasticity,* Arch. Rat. Mech. Anal., 94, 307–334 (1986).

[19] G. Francfort, F. Murat, L. Tartar, *Fourth Order Moments of a Non-Negative Measure on S^2 and Application,* to appear in Arch. Rat. Mech. Anal. (1995).

[20] L. Gibianski, A. Cherkaev, *Design of composite plates of extremal rigidity,* Ioffe Physicotechnical Institute preprint (1984). (English translation to appear in *Topics in the mathematical modeling of composite materials*, R.V. Kohn ed., series "Progress in Nonlinear Differential Equations and their Applications", Birkhauser, Boston.)

[21] Y. Grabovsky, R. Kohn, *Microstructures minimizing the energy of a two-phase elastic composite in two space dimensions II: the Vigdergauz microstructure,* to appear.

[22] Z. Hashin, *The elastic moduli of heterogeneous materials,* J. Appl. Mech., 29, 143–150 (1963).

[23] Z. Hashin, S. Shtrikman, *A variational approach to the theory of the elastic behavior of multiphase materials,* J. Mech. Phys. Solids, 11, 127–140 (1963).

[24] C. Jog, R. Haber, M. Bendsoe, *A displacement-based topology design method with self-adaptive layered materials, Topology design of structures*, Nato ASI Series E, M. Bendsoe et al. eds., 219–238, Kluwer, Dordrecht (1993).

[25] C. Jog, R. Haber, M. Bendsoe, *Topology design with optimized, self-adaptative materials,* Int. Journal for Numerical Methods in Engineeringm 37, 1323–1350 (1994).

[26] R. Kohn, G. Strang, *Optimal Design and Relaxation of Variational Problems I-II-III,* Comm. Pure Appl. Math., 39, 113–137, 139–182, 353–377 (1986).

[27] R. Lipton, *A saddle-point theorem with application to structural optimization,* J. Opt. Th. Appl., 81, 3, 549–567 (1994).

[28] P. Marcellini, *Approximation of quasi-convex functions, and lower semicontinuity of multiple integrals,* Manuscripta Mathematica, 51, 1–28 (1985).

[29] A. Michell, *The limits of economy of material in frame-structures,* Phil. Mag., 8, 589–597 (1904).

[30] H. Mlejnek, *Some explorations in the genesis of structures, Topology design of structures*, Nato ASI Series E, M. Bendsoe et al. eds., 287–300, Kluwer, Dordrecht (1993).

[31] F. Murat, *Contre-exemples pour divers problèmes où le contrôle intervient dans les coefficients,* Ann. Mat. Pura Appl., 112, 49–68 (1977).

[32] F. Murat, L. Tartar, *H-convergence,* Séminaire d'Analyse Fonctionnelle et Numérique de l'Université d'Alger, mimeographed notes (1978). (English translation to appear in *Topics in the mathematical modeling of composite materials*, R.V. Kohn ed., series "Progress in Nonlinear Differential Equations and their Applications", Birkhauser, Boston.)

[33] F. Murat, L. Tartar, *Calcul des Variations et Homogénéisation,* Les Méthodes de l'Homogénéisation Théorie et Applications en Physique, Coll. Dir. Etudes et Recherches EDF, Eyrolles, 319–369 (1985). (English translation to appear in *Topics in the mathematical modeling of composite materials*, R.V. Kohn ed., series "Progress in Nonlinear Differential Equations and their Applications", Birkhauser, Boston.)

[34] W. Prager, G. Rozvany, *Optimal layout of grillages,* J. Struct. Mech., 5, 1–18 (1977).

[35] G. Rozvany, M. Zhou, T. Birker, O. Sigmund, *Topology optimization using iterative continuum-type optimality criteria (COC) methods for discretized systems, Topology design of structures*, Nato ASI Series E, M. Bendsoe et al. eds., 273–286, Kluwer, Dordrecht (1993).

[36] K. Suzuki, N. Kikuchi, *A homogenization method for shape and topology optimization,* Comp. Meth. Appl. Mech. Eng., 93, 291–318 (1991).

[37] L. Tartar, *Estimation de coefficients homogénéisés,* Computing methods in applied sciences and engineering, R. Glowinski, J.L. Lions eds., Lecture Notes in Math., 704, Springer Verlag, 364–373 (1978).

[38] L. Tartar, *Estimations Fines des Coefficients Homogénéisés,* Ennio de Giorgi colloquium, P. Krée ed., Pitman Research Notes in Math., 125, 168–187 (1985).

[39] S. Vigdergauz, *Effective elastic parameters of a plate with a regular system of equal-strength holes,* Mech. Solids, 21, 162–166 (1986).

[40] M. Zhou, G. Rozvany, *The COC algorithm, Part II: Topological, geometrical and generalized shape optimization,* Comp. Meth. App. Mech. Engrg,. 89, 309–336 (1991).